Journal of Computational Neuroscience 16, 211–235, 2004

High Frequency Stimulation of the Subthalamic Nucleus Eliminates Pathological Thalamic Rhythmicity in a Computational Model

JONATHAN E. RUBIN
Department of Mathematics and Center for the Neural Basis of Cognition, University of Pittsburgh, Pittsburgh, PA 15260, USA

DAVID TERMAN
Department of Mathematics, The Ohio State University, Columbus, OH 43210, USA
terman@math.ohio-state.edu

Received September 5, 2003; Revised January 23, 2004; Accepted January 27, 2004

Action Editor: G. Bard Ermentrout

Abstract. Deep brain stimulation (DBS) of the subthalamic nucleus (STN) or the internal segment of the globus pallidus (GPi) has recently been recognized as an important form of intervention for alleviating motor symptoms associated with Parkinson's disease, but the mechanism underlying its effectiveness remains unknown. Using a computational model, this paper considers the hypothesis that DBS works by replacing pathologically rhythmic basal ganglia output with tonic, high frequency firing. In our simulations of parkinsonian conditions, rhythmic inhibition from GPi to the thalamus compromises the ability of thalamocortical relay (TC) cells to respond to depolarizing inputs, such as sensorimotor signals. High frequency stimulation of STN regularizes GPi firing, and this restores TC responsiveness, despite the increased frequency and amplitude of GPi inhibition to thalamus that result. We provide a mathematical phase plane analysis of the mechanisms that determine TC relay capabilities in normal, parkinsonian, and DBS states in a reduced model. This analysis highlights the differences in deinactivation of the low-threshold calcium T-current that we observe in TC cells in these different conditions. Alternative scenarios involving convergence of thalamic signals in the cortex are also discussed, and predictions associated with these results, including the occurrence of rhythmic rebound bursts in certain TC cells in parkinsonian states and their drastic reduction by DBS, are stated. These results demonstrate how DBS could work by increasing firing rates of target cells, rather than shutting them down.

Keywords: deep brain stimulation, basal ganglia, Parkinson's disease

1. Introduction

Deep brain stimulation (DBS) of the subthalamic nucleus (STN) or the internal segment of the globus pallidus (GPi) has recently gained great importance in the treatment of Parkinson's disease (PD) and other neurological disorders (for recent reviews and results, see e.g. Olanow et al., 2000; Benabid et al., 2001b,c; Gross, 2001; The Deep Brain Stimulation for Parkinson's Disease Study Group, 2001; Pollak et al., 2002). The basic mechanisms underlying DBS remain mysterious, however. It is not known whether DBS acts to enhance or suppress neuronal activity within a given structure, which areas and which neurons within these areas are acted upon by DBS, or how the geometry and orientation of neurons modulate the effect of the electric field

generated by the DBS. These issues present a daunting challenge for anyone seeking to determine how DBS improves motor symptoms.

There are several reasons why it has been believed that the primary action of DBS is to suppress neuronal activity. One argument is that because the clinical effects of DBS are similar to those of ablative surgeries, the mechanisms underlying these treatments must be similar (Benazzouz et al., 2000; Olanow et al., 2000, 2001; Benabid et al., 2001c). Experimental studies have demonstrated that in PD, the output nuclei of the basal ganglia, such as GPi, become overactive (Filion and Tremblay, 1991; Wichmann et al., 1999), thereby increasing the level of inhibition sent onto the thalamus. This may in turn inhibit the thalamus from passing along sensorimotor signals to the cortex. Ablative surgery clearly eliminates this over-activity; indeed, this is the explanation usually given for why it works. By analogy, one may expect that DBS of STN or GPi somehow has an inhibitory effect that reduces the increased activity of the GPi. This inhibitory effect may arise through a variety of mechanisms (Obeso et al., 2000; Benabid et al., 2001c,d; Beurrier et al., 2001; Levy et al., 2001; Wu et al., 2001).

A variety of recent experiments have called this viewpoint into question, however, by demonstrating that high-frequency stimulation (HFS) leads to enhanced activity in stimulated areas (Garcia et al., 2003) or downstream effects consistent with enhanced synaptic outputs from stimulated areas (Paul et al., 2000; Windels et al., 2000; Anderson et al., 2003; Hashimoto, 2003). This leads to a theoretical conundrum, as it is not at all clear how to explain the beneficial effects of DBS if its action is to enhance neuronal activity. As mentioned above, PD is associated with increased firing of GPi. If DBS enhances activity, then DBS would further increase the firing of GPi neurons. It seems contradictory to posit that DBS could ameliorate motor symptoms caused by an increase in GPi firing by further increasing this firing. *The goal of this paper is to demonstrate, with a computational model, why this is actually not contradictory, but rather is a natural consequence of the properties of the cells involved.*

It is crucial to note that the above arguments are phrased in terms of the firing rates of neurons. Several authors have pointed out that the *pattern* of neuronal activity, not just the rate, may be important (Bergman et al., 1994; Nini et al., 1995; Magnin et al., 2000; Montgomery et al., 2000; Obeso et al., 2000; Raz et al., 2000; Brown et al., 2001; Terman et al., 2001, 2002). In particular, numerous experimental studies have demonstrated that neurons within both the STN and GPi show an increased level of synchrony and bursting activity during parkinsonian states (Bergman et al., 1994; Nini et al., 1995; Magnin et al., 2000; Raz et al., 2000; Brown et al., 2001). Using a computational model, we show that while synchronous and patterned output of GPi (corresponding to a parkinsonian state) may disrupt the thalamic ability to relay depolarizing (e.g., sensorimotor) inputs, high-frequency, tonic output of GPi (corresponding to DBS) may restore thalamic relay capabilities.

Our computational model includes neurons within STN, GPe (external segment of globus pallidus), GPi, and the thalamus. While our focus is on modulation of thalamic firing by GPi, the interacting STN and GPe network is crucial in our model in that its signals (both from STN to GPi and from GPe to GPi) interact with intrinsic GPi currents to generate patterns of of GPi activity that are consistent with experimental data (DeLong, 1971; Filion and Tremblay, 1991; Wichmann et al., 1999; Raz et al., 2000; Hashimoto et al., 2003). We assume that the thalamus receives two sources of input. One input source is GPi, and the other corresponds to depolarizing signals, possibly relating to sensorimotor activity. Such signals can arrive at the thalamus via corticothalamic projections, for example. Here, we view the thalamus simply as a relay station whose role is to respond faithfully to incoming sensorimotor signals. In the discussion, we consider further the question of interaction of sensorimotor and basal ganglia inputs in the thalamus and the cortex.

We consider three states of the basal ganglia. In a "normal" state, output from GPi is irregular and uncorrelated. This has a minimal effect on the thalamic cells; in particular, the thalamus is able to transmit depolarizing signals accurately. In a "parkinsonian" state, GPi neurons fire bursts of action potentials at a tremor frequency of 3–8 Hz. The bursts are synchronized among subpopulations of GPi neurons. The resulting effect on thalamic cells is significant and the thalamus is no longer able to transmit depolarizing signals faithfully. Finally, we simulate DBS of STN neurons. We assume that DBS provides a high frequency, excitatory input to STN neurons. We find that this input leads to increased activity of STN neurons which in turn excite GPi cells, inducing them to fire tonically at high frequency. Our main result is that this can restore the ability of the thalamus to relay its sensorimotor input faithfully.

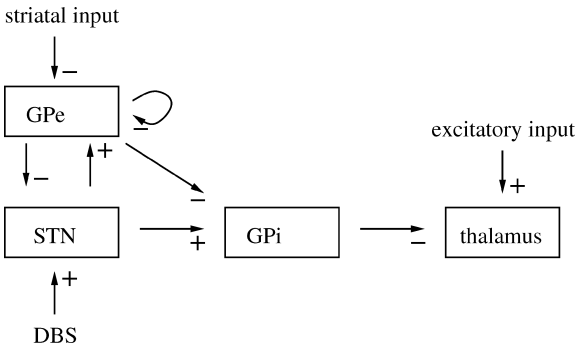

Figure 1. Structures included in the model network. Arrows with − signs indicate inhibitory synaptic connections and inputs, while arrows with + signs indicate excitatory synaptic connections and inputs. DBS denotes deep brain stimulation, which is applied to STN in some of our simulations.

2. Materials and Methods

2.1. The Network Model

The network model consists of four neuronal structures; these are the thalamus, STN, GPe and GPi. The network architecture is illustrated in Fig. 1. The thalamus receives synaptic inhibition from GPi and excitatory input, which we consider to relate to sensorimotor activity. GPi and GPe both receive excitatory input from STN, and GPe receives an applied current corresponding to input from the striatum. Moreover, there is interpallidal inhibition among the GPe neurons, and GPi receives inhibition from GPe. Finally, STN receives inhibition from GPe as well, and in some simulations it also is driven with a periodic applied current corresponding to high frequency stimulation (i.e., DBS). Precise details of connectivity and numbers of cells are described in the Appendix.

2.2. Model for Each Cell Type

Here we describe the computational model for each cell type. These are all single-compartment conductance-based biophysical models used in previous modeling studies. The precise forms of the nonlinear functions in the models and the parameter values are given in the Appendix.

We will denote variables and functions corresponding to cells within the thalamus, STN, GPe, and GPi with the subscript or superscript Th, Sn, Ge, and Gi, respectively. The synaptic current from structure α to structure β is denoted as $I_{\alpha\to\beta}$. The details of these currents are described in the Appendix.

Thalamic Neurons. Thalamic cells are modeled as:

$$\begin{aligned} C_m v'_{\mathrm{Th}} &= -I_{\mathrm{L}} - I_{\mathrm{Na}} - I_{\mathrm{K}} - I_{\mathrm{T}} - I_{\mathrm{Gi}\to\mathrm{Th}} + I_{\mathrm{SM}} \\ h'_{\mathrm{Th}} &= (h_\infty(v_{\mathrm{Th}}) - h_{\mathrm{Th}})/\tau_h(v_{\mathrm{Th}}) \\ r'_{\mathrm{Th}} &= (r_\infty(v_{\mathrm{Th}}) - h_{\mathrm{Th}})/\tau_r(v_{\mathrm{Th}}). \end{aligned} \tag{1}$$

Here, $I_{\mathrm{L}} = g_{\mathrm{L}}[v_{\mathrm{Th}} - E_{\mathrm{L}}]$, $I_{\mathrm{Na}} = g_{\mathrm{Na}} m_\infty^3(v_{\mathrm{Th}}) h_{\mathrm{Th}}[v_{\mathrm{Th}} - E_{\mathrm{Na}}]$, and $I_{\mathrm{K}} = g_{\mathrm{K}}[.75(1 - h_{\mathrm{Th}})]^4[v_{\mathrm{Th}} - E_{\mathrm{K}}]$ are leak, sodium, and potassium spiking currents, respectively, with square brackets denoting multiplication. Note that we use a standard reduction in our expression for the potassium current, which decreases the dimensionality of the model by one variable (Rinzel, 1985). In all the cell models we assume that the membrane capacitance C_m is unity. The current $I_{\mathrm{T}} = g_{\mathrm{T}} p_\infty^2(v_{\mathrm{Th}}) r_{\mathrm{Th}}[v_{\mathrm{Th}} - E_{\mathrm{T}}]$ is a low-threshold calcium current. This model is a simplification of a model in Sohal et al. (2002). Note that these model TC cells are at rest in the absence of inputs.

I_{SM} represents sensorimotor input to the thalamus and is modeled as a periodic step function of the form

$$\begin{aligned} I_{\mathrm{SM}} = i_{\mathrm{SM}} H(\sin(2\pi t/\rho_{\mathrm{SM}})) \\ \times [1 - H(\sin(2\pi(t + \delta_{\mathrm{SM}})/\rho_{\mathrm{SM}}))]. \end{aligned} \tag{2}$$

Here, H is the Heaviside step function, such that $H(x) = 0$ if $x < 0$ and $H(x) = 1$ if $x > 0$. Note that ρ_{SM} is the period of I_{SM}, i_{SM} is the amplitude, and δ_{SM} is the duration of positive input. In some simulations, we introduce noise into I_{SM}, eliminating its periodicity.

Firing properties of thalamic neurons are demonstrated in Fig. 2. In the plots there, $I_{\mathrm{Gi}\to\mathrm{Th}} = 0$ and $I_{\mathrm{SM}} =$ constant, except for several current injections. Observe from Fig. 2 that the thalamic cells are not spontaneously active. Moreover, as shown in the top panel, they respond to depolarizing input with continuous spiking. Larger applied currents elicit faster responses. Figure 2, bottom panel, demonstrates that the thalamic cells fire strong rebound bursts following release from sustained hyperpolarizing current (Zhan et al., 1999). A larger hyperpolarizing current leads to a stronger rebound. In what follows, the hyperpolarizing current will correspond to input from GPi and the rebound bursts correspond to tremor-like oscillations that may disrupt the flow of sensorimotor input through the thalamus.

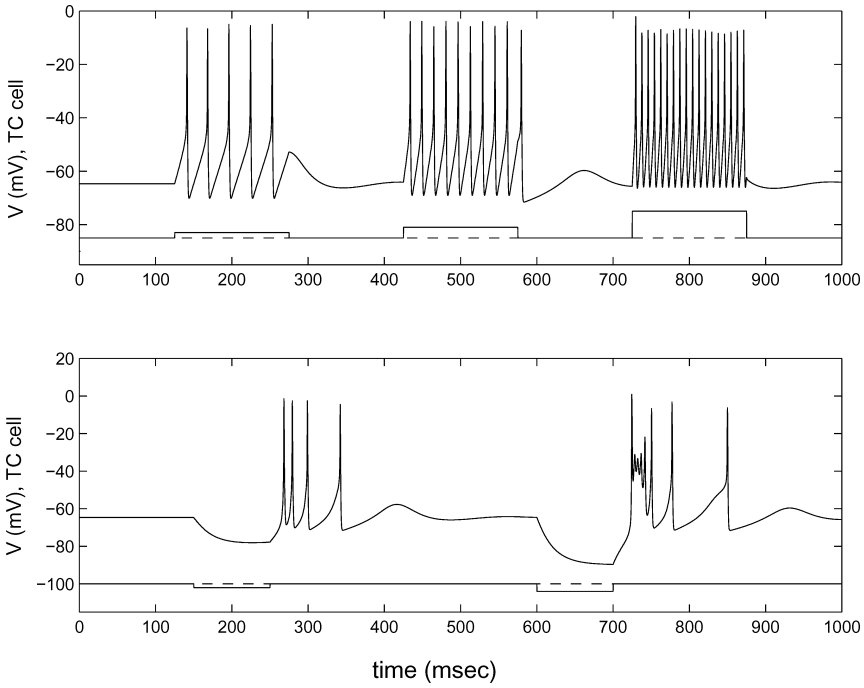

Figure 2. TC responses to depolarizing (top) and hyperpolarizing (bottom) input pulses. Note that TC cells here are at rest in the absence of inputs. In addition to TC voltage traces, the input is shown, shifted for visibility. The inputs $I_{\mathrm{Gi}\to\mathrm{Th}}$ (in pA/μm^2) are 2, 5, 10 (top) and $-.5$, -1 (bottom).

For Fig. 3, we assume that $I_{\mathrm{Gi}\to\mathrm{Th}}$ is constant and I_{SM} is a periodic function given by Eq. (2). In Fig. 3A, we take $I_{\mathrm{Gi}\to\mathrm{Th}} = 0$ and in Fig. 3B, we take $I_{\mathrm{Gi}\to\mathrm{Th}} = -1$, corresponding to hyperpolarizing input coming from GPi. We note that if $I_{\mathrm{Gi}\to\mathrm{Th}} = 0$, then thalamic cells faithfully follow periodic input I_{SM} over a wide range of input strength and frequency. This sensorimotor input would be relayed to the cortex.

If $I_{\mathrm{Gi}\to\mathrm{Th}} = -1$, then the thalamic response depends on the frequency of I_{SM}. The thalamic cells respond with bursting activity if I_{SM} is slow and with single action potentials if I_{SM} is sufficiently fast. This is shown in Fig. 3B; in the top (Fig. 3Bi) and bottom (Fig. 3Bii) figures, I_{SM} has a frequency of 10 Hz and 40 Hz, respectively. We note that burst responses of thalamic cells do not represent faithful relay of sensorimotor input to the cortex.

In order to understand why the thalamic response depends on the frequency of I_{SM} input, we note that the hyperpolarizing input $I_{\mathrm{Gi}\to\mathrm{Th}}$ tends to deinactivate the thalamic I_{T} current. If I_{SM} is sufficiently slow then I_{T} has enough time to deinactivate sufficiently so that thalamic cells respond with bursting activity. If I_{SM} is too fast, then I_{T} does not have enough time to deinactivate sufficiently and the thalamic cells respond with only one brief action potential.

STN Neurons. The voltage equation of STN neurons is of the form:

$$C_m v'_{\mathrm{Sn}} = -I_{\mathrm{L}} - I_{\mathrm{K}} - I_{\mathrm{Na}} - I_{\mathrm{T}} - I_{\mathrm{Ca}} - I_{\mathrm{Ge}\to\mathrm{Sn}} + I_{\mathrm{DBS}}. \tag{3}$$

This model was introduced in Terman et al. (2002). We make some parameter adjustments so that the STN cells display firing patterns more similar to those seen *in vivo*. A detailed description of the many parameters and nonlinear functions in the model is given in the Appendix. Note that I_{DBS} represents the input due to applied high frequency stimulation. This is discussed further in the Results.

Figure 4A and B shows the firing properties of the model STN neurons. These cells are intrinsically at a few Hz and exhibit high frequency sustained firing with sufficient excitatory input. They also display a prolonged delay before spiking resumes after sustained firing and strong rebound bursts after release from hyperpolarizing current.

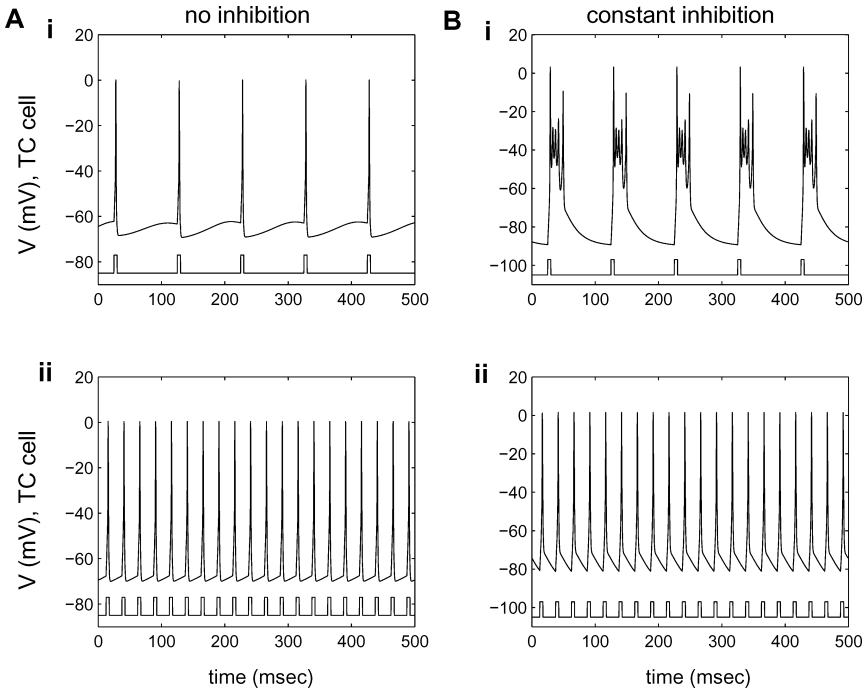

Figure 3. TC responses to periodic stimulation by depolarizing inputs. A: Responses in the absence of inhibitory input. B: Responses to a constant inhibitory current, which can lead to bursting. Here, $I_{\mathrm{Gi}\to\mathrm{Th}} = -1$. An individual model TC cell can respond faithfully over a wide range of input frequencies; 10 Hz (Ai and Bi) and 40 Hz (Aii and Bii) inputs are shown.

GPe and GPi Neurons. The voltage equation of GPe neurons is of the form:

$$C_m v'_{\mathrm{Ge}} = -I_{\mathrm{L}} - I_{\mathrm{K}} - I_{\mathrm{Na}} - I_{\mathrm{T}} - I_{\mathrm{Ca}} - I_{\mathrm{Sn}\to\mathrm{Ge}} - I_{\mathrm{Ge}\to\mathrm{Ge}} + I_{\mathrm{app}} \tag{4}$$

This model was also introduced in Terman et al. (2002), and as with the STN model, slight parameter adjustments have been made to reflect *in vivo* firing patterns. Here, I_{app} is a constant and represents input from the striatum. We model GPi neurons very similarly to GPe neurons, using a voltage equation of the form (4) but with Ge replaced with Gi; however, we renormalize certain parameters to reflect the fact that GPi neurons fire faster than GPe (DeLong, 1971; Filion and Tremblay, 1991; Raz et al., 2000; Hashimoto et al., 2003). Moreover, GPe and GPi cells receive different levels of striatal input (Gerfen and Wilson, 1996). We also assume that there is no inhibition from GPi cells to other GPi cells, but rather inhibition from GPe cells to GPi cells. Thus, the term $I_{\mathrm{Ge}\to\mathrm{Ge}}$ in Eq. (4) is replaced by $I_{\mathrm{Gi}\to\mathrm{Gi}}$ for GPi cells.

Figure 4C and D illustrates the firing properties of single GPe neurons. These cells can fire rapid periodic spikes with sufficient applied current. They also display bursts of activity when subjected to a small constant hyperpolarizing current, as well as an AHP following sustained firing. In our network model, phasic GPi firing requires phasic inhibitory inputs from GPe to GPi as would be delivered by such bursts, to interrupt the tonic firing of GPi that excitatory inputs from STN would otherwise help support.

2.3. *Synaptic Currents*

In each case, the synaptic current $I_{\alpha\to\beta}$ from structure α to structure β is given as

$$I_{\alpha\to\beta} = g_{\alpha\to\beta}[v_\alpha - E_{\alpha\to\beta}] \sum_j s_\alpha^j.$$

Here, $g_{\alpha\to\beta} > 0$ is the maximal synaptic conductance and $E_{\alpha\to\beta}$ is the synaptic reversal potential. The sum is over presynaptic cells. Each synaptic variable s_α^j satisfies a first order differential equation of the form

$$s'_\alpha = A_\alpha[1 - s_\alpha]H_\infty(v_\alpha - \theta_\alpha) - B_\alpha s_\alpha. \tag{5}$$

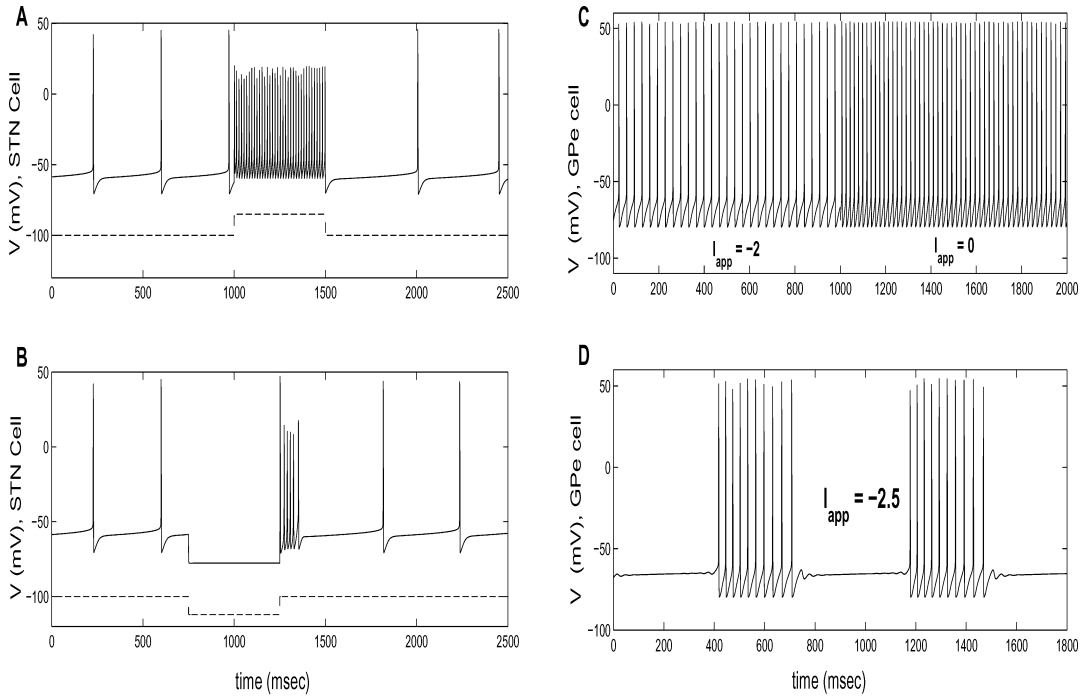

Figure 4. Voltage traces for STN and GPe neurons for different levels of applied current. A and B: STN neurons fire intrinsically at approximately 3 Hz and display high frequency sustained firing with higher input (as shown by the elevated dashed line). Here, $I_{\text{app}} = 50$. Note that there is a prolonged delay before subsequent firing after the elevated input is turned off. In B, observe that STN cells fire rebound bursts after release from hyperpolarizing current ($I_{\text{app}} = -30$). C and D: GPe neurons fire rapid periodic spikes under positive input. In D, observe that GPe cells fire bursts of spikes for small negative applied current.

H_∞ is a smooth approximation of the Heaviside step function. Note that A_α and B_α control the synaptic time courses; these are not simply instantaneous switches.

2.4. *Noise*

In some simulations, we introduce noise into the time intervals between sensorimotor inputs. We consider time intervals selected from a uniform distribution, with minimum interval 35 msec and maximum interval 80 msec, and from a Poisson distribution, with an enforced minimum interval of 10 msec. The latter is achieved by computing each interval duration as $10 - \log(ran(1))/.03$ where $ran(1)$ is a random number selected from a uniform distribution on [0, 1].

We compute an error index to measure the reliability and accuracy with which cells respond to sensorimotor inputs. An index of 0 corresponds to optimal performance, in which no errors are made. This corresponds to one output spike for each sensorimotor input. The error index equals the total number of errors divided by the total number of input stimuli. Two types of errors are counted: false positives and misses. False positives consist of spikes with no corresponding stimulus as well as multiple spikes in response to a single stimulus. Misses are failures to respond within 10 msec of a stimulus.

2.5. *Simulations*

Simulations were performed on personal computers using the software XPP (Ermentrout, 2002). The numerical method used was an adaptive-step fourth order Runge-Kutta method (QualSt.RK4 in XPP), with a typical time step of 0.1 msec.

3. Results

3.1. *Normal and Parkinsonian States*

Our main objective is to study how thalamic cells respond to excitatory signals, perhaps representing

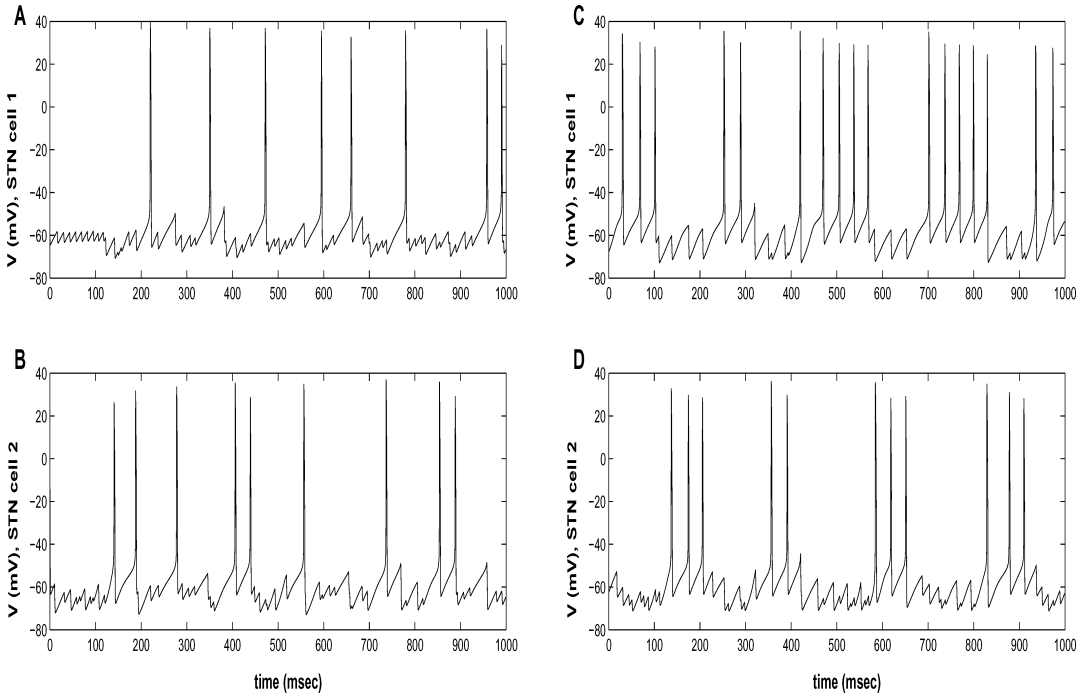

Figure 5. Normal and parkinsonian states. A and B: During the normal state, STN neurons fire irregularly and there is little correlation between the activities of different neurons. C and D: During the parkinsonian state, each STN neuron fires in a periodic tremor-like fashion. The entire population of STN neurons breaks up into two clusters; neurons within each cluster are synchronized and neurons in different clusters fire out-of-phase. One STN neuron from each cluster is shown here. The GPe cells fire in a similar manner.

sensorimotor input, during both "normal" and "parkinsonian" states. Here we define what is meant by each of these states.

As shown by Plenz and Kitai (1999), the STN and GPe neurons form an excitatory/inhibitory network that can oscillate in the absence of input from other structures. In Terman et al. (2002), we describe several different types of activity patterns that may be generated by the isolated model STN/GPe network (but with a constant level I_{app} of striatal inhibition to GPe), along with a detailed description of how the activity patterns depend on parameters. We demonstrate that this network can produce both irregular asynchronous activity and synchronous tremorlike activity as shown in Fig. 5. We note that both of the patterns shown in Fig. 5 are generated for a network with exactly the same architecture. In order to switch from the irregular pattern to the synchronous pattern, we increased I_{app} and decreased $g_{\text{Ge}\to\text{Ge}}$. These parameters correspond to the level of striatal input to GPe and interpallidal inhibition, respectively. Note that experimental results show an increase in striatal inhibition to GPe (e.g., Albin et al., 1989) and a decrease in intrapallidal inhibition (Stanford et al., 1999; Ogura et al., 2000) in parkinsonian conditions.

By a "normal state", we mean that the parameters are chosen so that the STN/GPe network produces the irregular pattern shown in left panels of Fig. 5. By a "parkinsonian state", we mean that the parameters are chosen so that the STN/GPe network produces the more regular, synchronous activity shown in right panels of Fig. 5. These definitions are based on experimental results revealing corresponding patterns under normal versus parkinsonian conditions (Bergman et al., 1994; Nini et al., 1995; Magnin et al., 2000; Raz et al., 2000; Brown et al., 2001).

3.2. DBS Off

Figures 6 and 7 illustrate the behavior of the full network during the normal and parkinsonian states, respectively, when there is no DBS. During the normal state, the thalamus responds faithfully to the excitatory sensorimotor input. In this case, the uncorrelated, irregular input from GPi, while occurring at a high

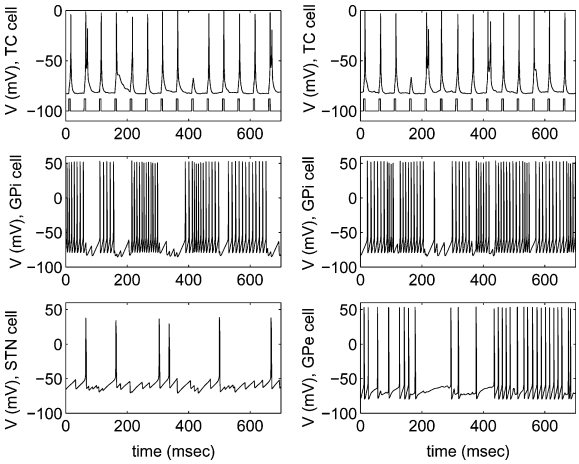

Figure 6. Voltage traces for two typical TC cells (top), GPi cells (middle), and an STN and GPe cell (bottom) in a normal state. In the top plot, the pattern of sensorimotor input is displayed beneath the TC voltage. The TC cell faithfully transmits this input to the cortex.

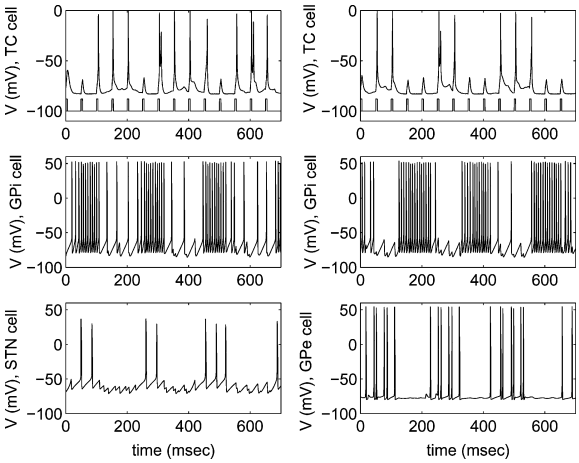

Figure 7. Voltage traces for two typical TC cells (top), GPi cells (middle), and an STN and GPe cell (bottom) in a parkinsonian state. In the top plot, the pattern of sensorimotor input is displayed beneath the TC voltage. The TC cell is unable to relay this input faithfully to the cortex.

frequency, does not disrupt thalamic relay. The firing pattern of typical GPi cells sending input to the TC cells shown appear in the middle row of the plot. A measure of the synaptic input from GPi to TC in the normal state is displayed in Fig. 9A.

On the other hand, during the parkinsonian state, the thalamus is no longer able to relay sensorimotor input faithfully. The synchronous, bursting output of GPi is now powerful enough to influence thalamic activity, and this is clearly reflected in both the thalamic responses in Fig. 7 and in the synaptic input time course in Fig. 9B. Note from the top two rows of Fig. 7 that thalamic responsiveness is particularly compromised during phases of intense GPi activity. The phasic GPi firing here is shaped largely by the phasic GPe bursts, also shown in Fig. 7, without which the GPi cells would fire more tonically.

3.3. DBS On

We now introduce deep brain stimulation (DBS) of the STN. We model this as

$$I_{\mathrm{DBS}} = i_D H(\sin(2\pi t/\rho_D)) \times [1 - H(\sin(2\pi(t+\delta_D)/\rho_D)], \qquad (6)$$

where i_D corresponds to stimulation amplitude, ρ_D to stimulation period, and δ_D to the duration of each impulse. In Fig. 8, the same parameters are used as in the parkinsonian state simulation shown in Fig. 7, but DBS is now applied, with $i_D = 200$, $\rho_D = 6$ msec, and $\delta_D = 0.6$ msec. Note that DBS completely restores the thalamic ability to transmit sensorimotor information. The corresponding input from GPi to TC is shown in Fig. 9C. If DBS is removed, then the loss of faithful relay seen in Fig. 7 quickly returns.

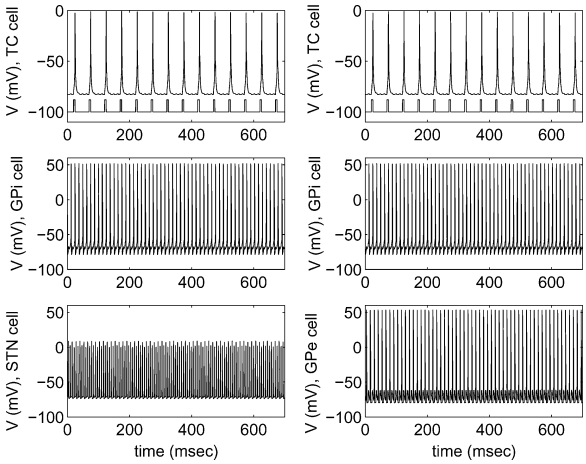

Figure 8. Voltage traces for two typical TC cells (top), GPi cells (middle), and an STN and GPe cell (bottom) with DBS applied. In the top plot, the pattern of sensorimotor input is displayed beneath the TC voltage. Although the network parameters are set to produce the parkinsonian state in the absence of DBS, the presence of DBS restores the faithful relay of inputs to the cortex by the TC cell.

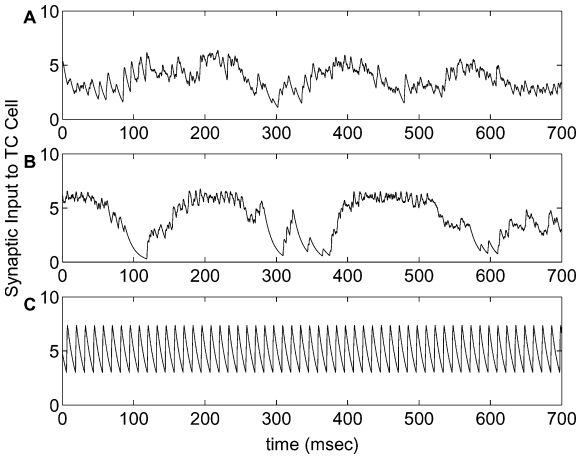

Figure 9. Total synaptic input from GPi received by a TC cell in normal (A), parkinsonian (B), and DBS (C) simulations. The synaptic input is computed as the sum of the synaptic conductances over the eight GPi cells projecting to the TC cell.

3.4. Robustness

The differential TC responsiveness to sensorimotor stimulation under normal, parkinsonian, and DBS conditions is robust with respect to noise in the input time course. In Fig. 10A and B, we show examples of the voltage of a typical TC cell, together with the pattern of inputs received, under these three conditions, after the introduction of stochasticity in the time interval between inputs. In Fig. 10A, we show results with time intervals selected from a uniform distribution with minimum interval 35 msec and maximum interval 80 msec. Figure 10B displays results with time intervals selected from a Poisson distribution with an enforced minimum interval of 10 msec (see Section 2). In all cases, parkinsonian conditions induced missed spikes and excess bursting in TC cells, while DBS restores the TC responsiveness to sensorimotor inputs that is compromised by parkinsonian conditions.

In Fig. 10C, the extent to which TC firing reflects the pattern of inputs to the TC cells is quantified under the uniform input interval distribution. The boxplots were generated from 20 trials of 2000 msec each, for each network state. The normal case actually produces the fewest misses in general, but it gives rise to a greater error index than the DBS case because it features more instances of multiple spikes being fired in response to single stimuli (as can be seen in the example in Fig. 10A). It is interesting to note that performance of DBS under noisy input conditions declines if the intensity of DBS becomes too strong (data not shown) or the input frequency becomes too great.

We also tested the effect of DBS for different levels of DBS frequency, amplitude and pulse widths. Representative results are displayed in Fig. 11. For various DBS parameters in Eq. (6), we plot the number of correct responses, out of a maximum of 20, made over a one second interval during which a 20 Hz excitatory sensorimotor input, given by Eq. (2), arrives at the thalamus. Correct responses are defined as single spikes fired by a thalamic cell; when the cell bursts or fails to spike, the result is not counted. Results are averaged over two thalamic cells to produce each data point. When the amplitude of DBS is sufficiently large, the DBS improves thalamic relay of sensorimotor input over a wide range of DBS input durations (i.e., pulse widths) and frequencies, although we omit most of the corresponding curves from Fig. 11 for clarity.

Rizzone et al. (2001) systematically studied DBS effectiveness, in terms of clinical evaluation of motor symptoms, as a function of stimulation duration and rate. In brief, they found that increasing stimulation rate (i.e., decreasing the period) or increasing the stimulation duration lowered the stimulation amplitude needed to attain clinical benefit, although not all of their results were statistically significant. Figure 11 shows that in our results, the peak in correct responses indeed occurs at lower $i_{\mathrm{DBS}} = i_D$ as $ddbs = \delta_D$ is increased from 0.15 to 0.3 to 0.6 msec, although at high enough stimulation intensity, even small DBS durations lead to some improvements. Further, DBS efficacy significantly drops if the stimulation frequency becomes too low, although this dependence is nonmonotonic. Interestingly, stimulation at quite low frequencies ($\rho_D = pdbs = 40$ msec, corresponding to 25 Hz) actually diminishes thalamic relay capabilities, relative to the unstimulated case. This occurs because parkinsonian-like STN and GPe bursts still occur with 25 Hz stimulation, but they become longer, leading to prolonged phases of strong inhibition from GPi to TC cells.

4. Analysis

4.1. Introduction

We use geometric phase plane methods to gain insight into the numerical results presented in the previous section. In this analysis, we consider how one model thalamic cell responds to combinations of inhibitory GPi and excitatory sensorimotor inputs. We consider three

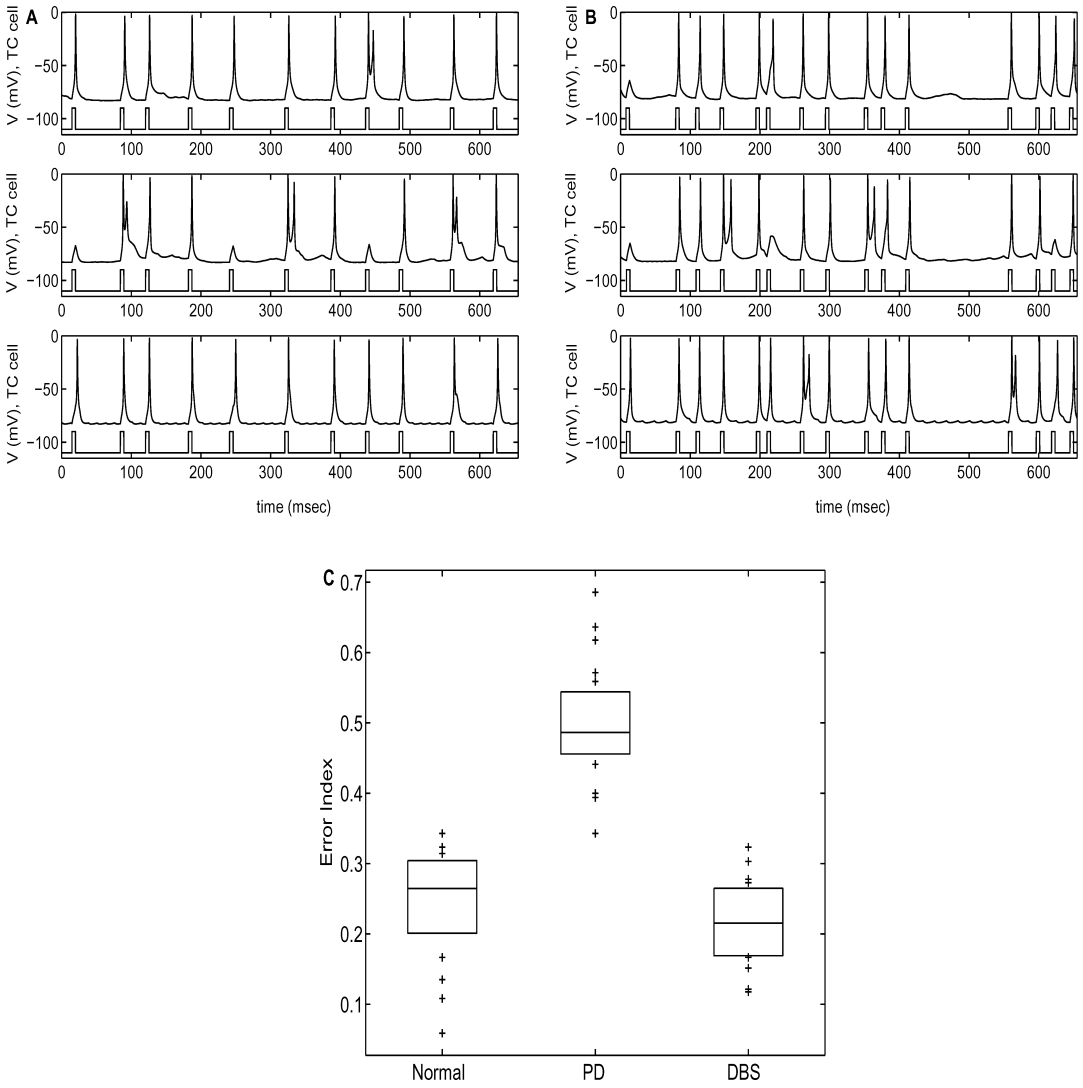

Figure 10. Thalamic responses to noisy sensorimotor inputs. A and B: TC voltage versus time, with the input pattern displayed underneath. A: Results with time intervals between inputs selected from a uniform distribution under normal (top), parkinsonian (middle), and DBS (bottom) conditions. B: Results with time intervals from a Poisson distribution under the same three conditions. In each of A and B, the same noisy input is shown for all three conditions, for fairness of comparison. C: Relative numbers of errors made in the three different conditions, with uniform interstimulus intervals, based on 20 trials of 2000 msec each in each condition. The boxes show the median, 25th percentile, and 75th percentile levels of the error index for the 20 trials in each case, while markers show the outlying values that occurred.

classes of GPi input; these shall be referred to as the *normal*, *parkinsonian*, and *DBS* cases.

For clarity of analysis, we first consider a model thalamic cell that satisfies a reduced version of Eq. (1) given by

$$\begin{aligned} v' &= -(I_{\mathrm{L}} + I_{\mathrm{T}})/C_{\mathrm{Th}} - I_{\mathrm{Gi}\to\mathrm{Th}} + I_{\mathrm{SM}} \\ w' &= \phi(w_\infty(v) - w)/\tau_h(v) \end{aligned} \tag{7}$$

Here, we have dropped the subscript *Th* in our dependent variables and write the T-current inactivation variable as w. The other notation is as in (1). The sensorimotor input, I_{SM}, is given by (2) with period $\rho_{\mathrm{SM}} \approx 50$ msec and duration $\delta_{\mathrm{SM}} \approx 7$ msec, unless otherwise noted. We model the GPi input as

$$I_{\mathrm{Gi}\to\mathrm{Th}} = g_{\mathrm{Gi}\to\mathrm{Th}} s_{\mathrm{Gi}} [v - E_{\mathrm{Gi}\to\mathrm{Th}}] \tag{8}$$

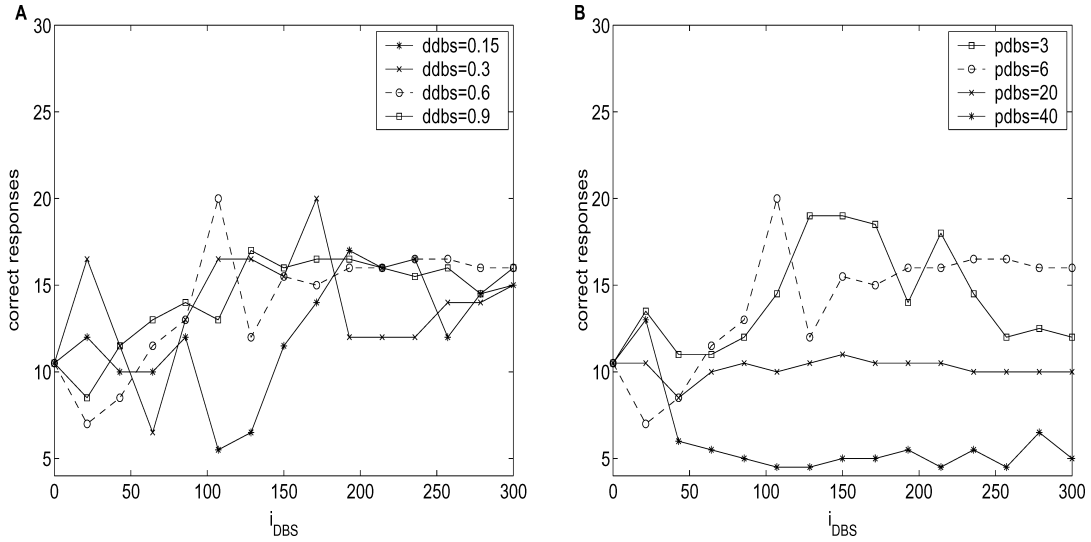

Figure 11. Response of thalamic cells to sensorimotor input for different DBS parameters. A and B: Average thalamic correct responses, out of a possible total of 20, are shown as a function of the amplitude (i_D) of DBS. A: DBS stimulus duration (ddbs, in msec) is varied, with pdbs = 6 msec. B: DBS period (pdbs, in msec), is varied, with ddbs = 0.6 msec. Note that the case of pdbs = 6 msec and ddbs = 0.6 msec appears as the dashed curve with 'o' data points in both plots.

where $s_{\text{Gi}} = s_{\text{Gi}}(t)$ is now a prescribed, time-dependent function. For convenience, we introduce the notation $s(t) \equiv s_{\text{Gi}}(t)$. We shall see that this reduced thalamic model yields qualitatively similar responses to the thalamic responses generated by the full network model.

We select the form of $s(t)$ based on the pattern of inhibition from GPi to the thalamus in the full network simulations, as displayed in Fig. 9. For the *normal* case, we take $s(t)$ to be a small positive constant. That is, we assume that during the normal case, the influence of GPi on thalamic activity is roughly constant over time. This is because GPi neurons fire in an irregular and uncorrelated manner. Note that the top panel of Fig. 9 shows the summed synaptic conductance over just eight uncorrelated GPi inputs to a TC cell; with a larger GPi population, irregular firing will translate into an approximately constant synaptic input.

For the *parkinsonian* case, we take $s(t)$ to be a periodic square-wave, given by the equation

$$s(t) = H(\sin(2\pi t/\rho_I))[1 - H(\sin(2\pi(t + \delta_I)/\rho_I)], \tag{9}$$

with period $\rho_I \approx 400$ msec and duration $\delta_I \approx 150$ msec. Here, we are assuming that during the parkinsonian case, output from GPi is synchronous with a tremor-like frequency, as seen in the middle row of Fig. 7, and generates rhythmic bursts of inhibition, as in Fig. 9. Note that while we exaggerate the period ρ_I and duration δ_I slightly in this section to clarify the presentation, qualitatively identical effects occur with shorter ρ_I, δ_I, as in Figs. 7 and 9.

Finally, for the DBS case, we take $s(t)$ is be a positive constant, as in the normal case but of a larger magnitude. Here, we are assuming that DBS results in a continuous tonic firing of GPi and a roughly constant, elevated inhibition, as seen in the middle row of Fig. 8 and in Fig. 9, respectively.

4.2. *Phase Planes—Constant Input*

The uncoupled model thalamic cell satisfies the pair of first-order ordinary differential equations given in (7). The phase plane provides a powerful method for understanding properties of solutions and analyzing how solutions depend on different combinations of inputs. We introduce this method by first assuming that both inputs to the thalamic cell are constant and time-independent. That is, here we assume that $I_{\text{SM}} \equiv I_*$, a constant, and $I_{\text{Gi}\to\text{Th}}$ is given by (8), with $s_{\text{Gi}} \equiv s_*$, another constant, although $I_{\text{Gi}\to\text{Th}}$ does still depend on v. In the subsections that follow, we consider the case of time-varying sensorimotor and pallidal inputs.

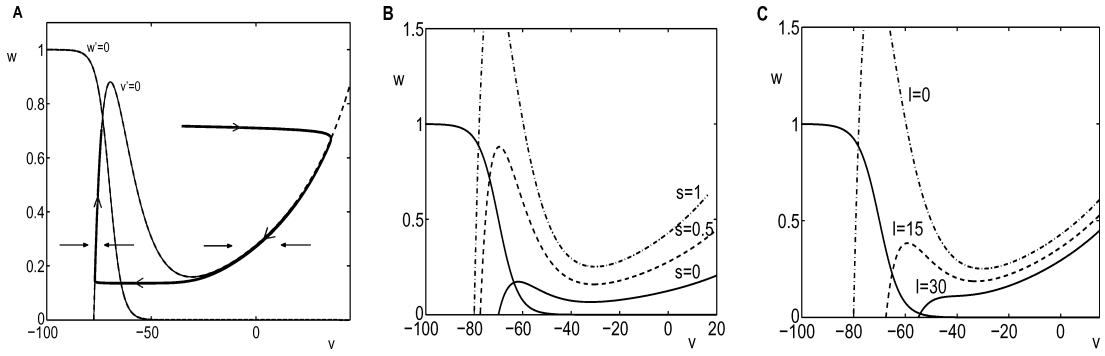

Figure 12. Nullclines for the reduced thalamic model. A: The thin arrows off of the nullclines illustrate that solutions to (7) are attracted to the left and right branches of the v-nullcline. The bold curve shows the response to a depolarizing input. This trajectory follows the v-nullcline for most of its duration, on its way to the rest state where the two nullclines intersect. The arrowheads along this trajectory show the directions along which v and w evolve as time advances. B: The w-nullcline is shown along with 3 different v-nullclines with $g_{\mathrm{Gi}\to\mathrm{Th}} = 0.8$ and $I_* = 0$, each corresponding to a different value of s_* as labeled (solid: $s_* = 0$, dashed: $s_* = 0.5$, dash-dotted: $s_* = 1$). C: The w-nullcline is shown along with 3 different v-nullclines with $g_{\mathrm{Gi}\to\mathrm{Th}} = 0.8$ and $s_* = 1$, each corresponding to a different value of I_* as labeled (solid: $I_* = 30$, dashed: $I_* = 15$, dash-dotted: $I_* = 0$).

First suppose that $I_* = 0$ and $s_* = 0.5$. The phase plane for this system is shown in Fig. 12. The v-nullcline, namely the curve where $v' = 0$, is a cubic-shaped curve and the w-nullcline, where $w' = 0$, is a curve that decreases as v increases; these are dashed in Fig. 12A. Solutions to (7) that start away from the v-nullcline are initially attracted toward the left and right branches of the v-nullcline when ϕ is small, as indicated by the thin arrows in Fig. 12A. There is also an attracting point where the two nullclines intersect. This corresponds to the rest state of the cell (with $I_* = 0$ and $s_* = 0.5$ fixed), toward which all trajectories tend. We shall make the biologically accurate assumption throughout the analysis that ϕ is a small parameter. That is, w, corresponding to deinactivation of the I_{T}-current, evolves on a slower time scale than the membrane potential v. With this assumption, the solutions to (7) that we shall analyze spend most of their time near the v-nullcline.

The bold curve in Fig. 12A shows the response of the cell to a fictitious input, which depolarizes the cell from the rest state to a voltage of -40 mV, generated by simulation of (7) with small, positive ϕ. At first voltage increases quickly, although the rate of increase cannot be seen from the figure shown. Next, there is an active phase, during which voltage slowly decreases along with w as the T-current inactivates. During the active phase, the trajectory lies close to the right branch of the cubic v-nullcline. Eventually, the solution approaches the right knee of the v-nullcline. At this point, w levels off, while v continues to decay. Finally, the T-current begins to deinactivate, such that w increases (and v increases slightly as well). This last stage is the silent phase, and during the silent phase the trajectory lies close to the left branch of the v-nullcline. Note that although the solutions cannot actually lie on the v-nullcline when $\phi > 0$, the trajectory still travels very near the left and right branches of the cubic nullcline silent and active phases, respectively. In what follows, we will refer to solutions as lying on various nullclines.

We next consider how the phase plane changes with respect to I_* and s_*. Both of these constants appear in the v-equation, so changing them changes the v-nullcline. The w-nullcline does not change under changes of these parameters. The v-nullclines for different values of I_* and s_* are shown in Fig. 12B and C. Note that increasing I_* lowers the v-nullcline while increasing s_* raises the v-nullcline. This reflects the fact that I_* corresponds to an excitatory input, while s_* represents an inhibitory synaptic input. Note also from Eq. (8) that s_* multiplies the v-dependent term $(v - E_{\mathrm{Gi}\to\mathrm{Th}})$ in the v-equation; thus, decreases in s_* and increases in I_* do not have exactly the same effect on the v-nullcline.

The relative positions of nullclines for different levels of s and I determine the responses of the TC cells during our simulations. Suppose that a thalamic cell receives a level of inhibition s_* and that (v, w) are such that the trajectory for this cell lies on the left branch of the corresponding nullcline. The key question is, what happens when that cell receives an excitatory input of strength I_*, which lowers its nullcline? The

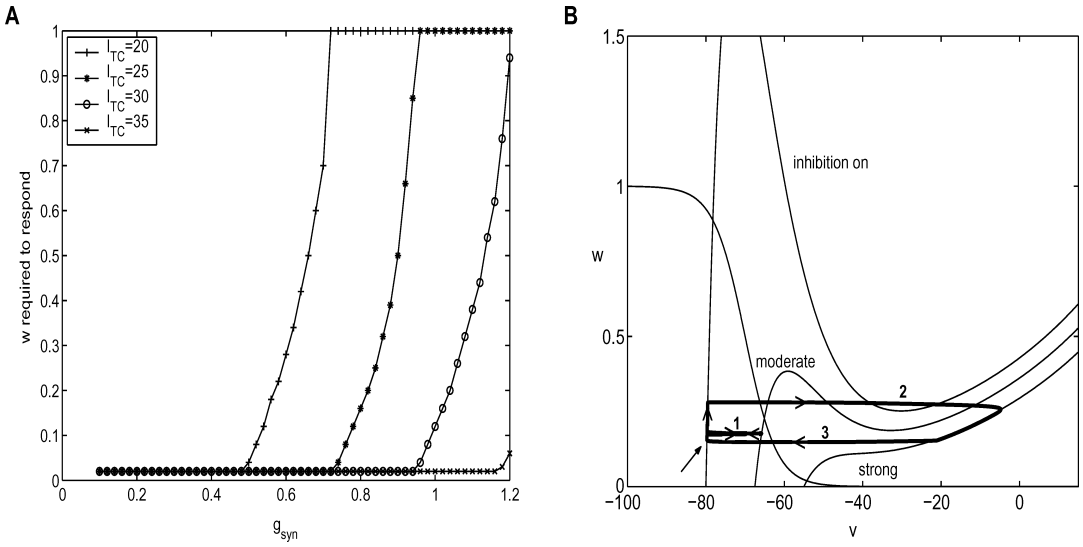

Figure 13. Availability of I_T determines TC responses to excitatory inputs. A: The minimum level of w needed for a reduced thalamic cell, initially at a fixed voltage, to fire a spike in response to an excitatory input, as a function of a constant level of synaptic inhibition to the cell ($g_{syn} = g_{Gi\to Th}s_*$) and the strength $I_* = I_{TC}$ of the input. When a curve reaches $h = 1$, this means that the TC cell will not respond to the corresponding excitatory input when subjected to the given level of inhibition, regardless of T-current availability. B: A trajectory of (7) in the (v, w) phase space, with inputs evolving as described in the text. The three nullclines are the same ones shown in Fig. 12C. The starting position of the trajectory is marked with an arrow; this is also the ending position of the trajectory.

answer depends on the level of w, corresponding to the availability of the T-current. Figure 13A shows that for fixed inhibitory input s_*, a larger w is required to spike in response to weaker inputs (smaller I_*), as expected from Fig. 12C. As s_* increases, for fixed I_*, a greater w is required to respond, as expected from Fig. 12B.

This point is illustrated more dynamically in Fig. 13B. This figure shows the same three nullclines featured in Fig. 12C, corresponding to $g_{Gi\to Th}s_* = 0.8$ and different levels of I_*, and a trajectory that jumps between the nullclines. At first, the cell receives no excitatory input ($I_* = 0$) and thus lies on the "inhibition" nullcline, near $v = -80$ and $w = 0.2$, as marked by the arrow in Fig. 13B. A moderate strength ($I_* = 15$) excitatory input is introduced. This causes the relevant nullcline to become the one labeled "moderate" in the figure. The trajectory jumps to this nullcline, traveling along **1**, but it lands on the left branch again, because w is not large enough for a response to this level of input. In terms of nullclines, we observe in Fig. 13B that the trajectory lands below the left "knee" of the "moderate" nullcline. The input is removed and the trajectory returns to the "inhibition" nullcline, essentially moving back along **1** because w did not change very much while the input was on. On the "inhibition" nullcline, w slowly rises, corresponding to slow T-current deinactivation. Next, a strong ($I_* = 30$) excitatory input is introduced. Although the trajectory lies below the knee of the "moderate" nullcline, and thus would not have responded to a moderate input (not shown), it is above the knee of the "strong" nullcline and thus jumps up to the right branch of the "strong" nullcline along **2**, reaching this branch near $v = -5$ and $w = .25$. Finally, when the strong input is removed, the trajectory jumps back along **3** to the "inhibition" nullcline, landing back near its starting point (the arrow in Fig. 13B).

In summary, a reduced model TC cell can respond to an excitatory input if its position in phase space, determined by availability of I_T, lies above the knee of the cubic $v' = 0$ nullcline, determined jointly by the strength of the arriving input and the current level of inhibition to the TC cell.

4.3. Normal Case

We now consider the normal case in which $I_{Gi\to Th}$ is a small constant and there is time-dependent sensorimotor input given by the periodic step-function (2). The voltage traces corresponding to (7) for this case are shown in the top row in Fig. 14A and B. Note that the thalamic cell reliably follows the

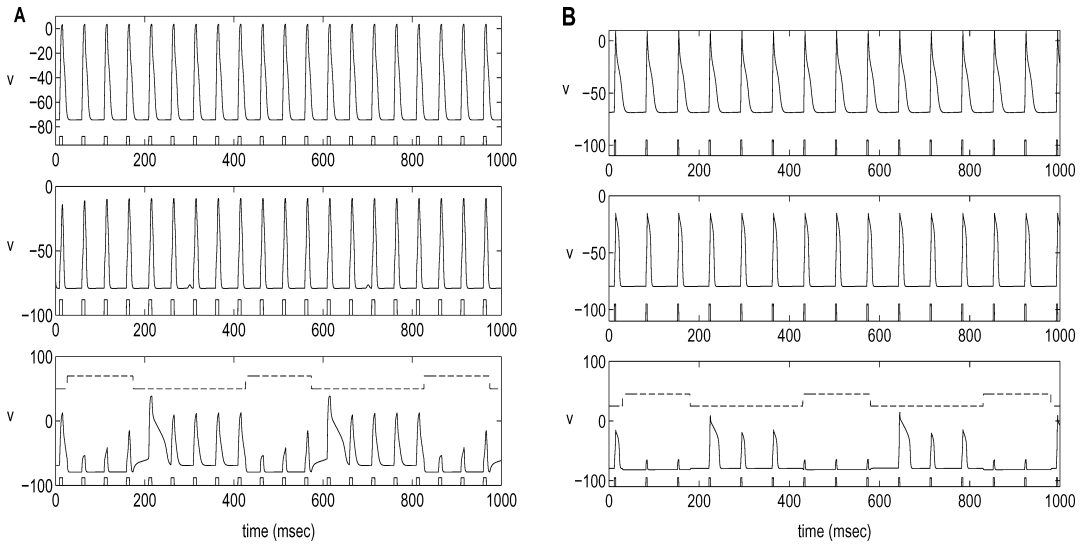

Figure 14. Voltage traces for a reduced TC cell in response to excitatory sensorimotor inputs, with inhibition corresponding to normal (top), DBS (middle), and parkinsonian (bottom) states. The pattern of sensorimotor input is displayed beneath each voltage trace. Parameters of I_{SM} in Eq. (2) are A: $i_{SM} = 25$, $\rho_{SM} = 50$, $\delta_{SM} = 7$; B: $i_{SM} = 30$, $\rho_{SM} = 70$, $\delta_{SM} = 3$. The inhibition to the TC cell in the parkinsonian case, multiplied by a constant for visibility, is displayed as the dashed line above the bottom voltage traces.

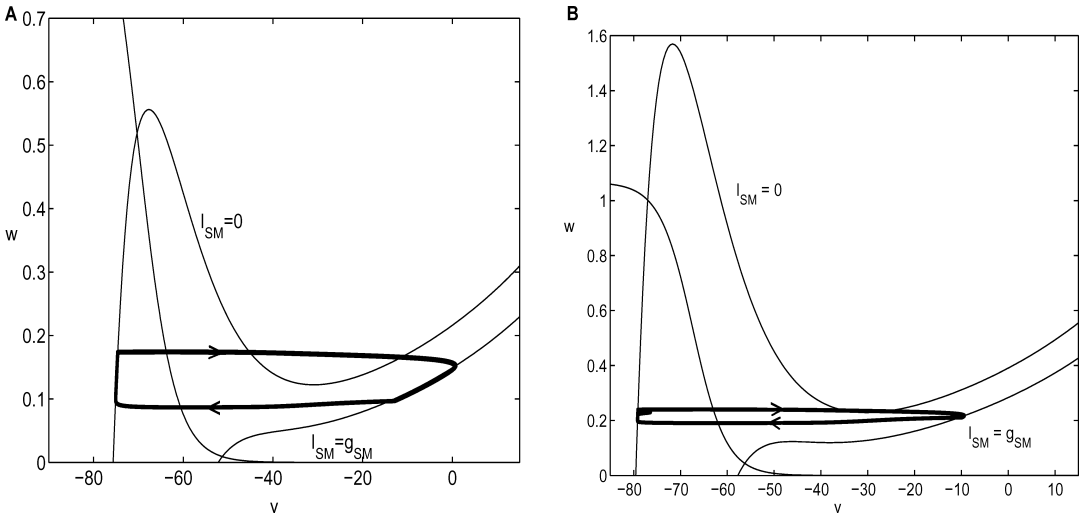

Figure 15. Thalamic oscillation in the phase plane in response to excitatory inputs in the normal (A) and DBS (B) cases, with parameters of I_{SM} as in Fig. 14A. A: w versus v for the solution shown in the top panel of Fig. 14A. B: w versus v for the solution shown in the middle panel of Fig. 14A.

sensorimotor input (shown below the voltage trace, for comparison).

The projection of the solution onto the phase plane is shown in Fig. 15A. There are now two cubic nullclines to consider, depending on whether $I_{SM} = 0$ or $I_{SM} = g_{SM} > 0$, both with $s(t)$ given by a small positive constant. During the silent phase, the solution lies along the left branch of the $I_{SM} = 0$ cubic. This continues until I_{SM} switches to g_{SM} and the solution jumps up to the right branch of the $I_{SM} = g_{SM}$ cubic. The solution jumps down to the silent phase after I_{SM} switches back to 0. If the trajectory is below the right knee of the $I_{SM} = 0$ cubic when this occurs, then the jump down is immediate (as shown); if not, then the jump down

occurs after a period in which the trajectory lies along the right branch of the $I_{SM} = 0$ cubic (not shown). The latter case will occur with shorter excitatory input duration, for example. No matter which of these possibilities occurs, the solution eventually lies along the left branch of the $I_{SM} = 0$ cubic and this process then repeats.

We note that when the solution jumps up to the active phase, it lies well *above* the left knee of the $I_{SM} = g_{SM}$ cubic. If this were not the case—that is, if the solution lay *below* this left knee—then the solution would jump up to the *left* branch of the I_{SM} cubic; that is, the solution would remain in the silent phase and not respond to the sensorimotor input, as illustrated in Fig. 13B. In the normal case, however, this is extremely rare, due to the irregularity and non-rhythmicity of the GPi inhibition to the thalamus in this case.

4.4. DBS Case

We next consider the DBS case. We assume that $s(t) = s_*$, a large positive constant, and the sensorimotor input is again given by (2). The resulting voltage traces are shown in the middle rows of Fig. 14A and B. Note that the thalamus does an excellent job in following the sensorimotor input.

The analysis of this case is similar to that discussed in the preceding subsection. There are two cubics to consider, depending on whether $I_{SM} = 0$ or $I_{SM} = g_{SM}$, both defined with $s = s_*$, a larger constant than in the normal case. The solution trajectory lies along the left branch of the $I_{SM} = 0$ cubic during the silent phase and along the right branch of the $I_{SM} = g_{SM}$ cubic during the active phase. These nullclines along with the projection of the solution onto the phase plane are shown in Fig. 15B. Note that while the trajectory in this case is quite similar to the normal case appearing in Fig. 15A, the two figures have different vertical scales, and the w values are higher in the DBS scenario. This reflects a greater availability of I_T resulting from a stronger inhibitory input.

We have also tested the reduced model with time-varying inhibitory input, representing time-dependent GPi responses to high frequency stimulation. While the trajectory jumps rapidly between the left branches of the inhibition-on and inhibition-on nullclines, the TC cell is again always able to respond to incoming excitatory input (data not shown). Finally, we note that if the strength s_* of inhibition is made strong enough, the TC cell responses can be blocked, even in the presence of DBS, as indicated in Fig. 13A.

4.5. Parkinsonian Case

Finally, we consider the parkinsonian case. The GPi input is modeled as (8) with $s(t)$ given by (9). For illustrative purposes, we set the value of $s(t)$ to become positive approximately every 400 msec, which is a bit slower than tremor frequency, and $s(t)$ remains positive for approximately 150 msec during each cycle. The sensorimotor input is modeled as (2), as in the other cases.

The resulting voltage trace is shown in the bottom row of Fig. 14A and B, along with $s(t)$, multiplied by a constant and shifted up for visibility. Note that the thalamus does not fire in response to every sensorimotor input. Further, the failed TC responses occur while the TC cell is receiving inhibition.

The projection of the solution for the reduced system is shown in Fig. 16. The first four peaks in v in the bottom row of Fig. 14A give rise to corresponding structures in Fig. 16A, and these are labeled in Fig. 16A according to the chronological order in which they occur in Fig. 14A. Figure 16B shows the same voltage trace, with the peaks labeled, and the corresponding time course of w appears in Fig. 16C. There are now potentially four nullclines to consider; these depend on whether $s(t) = s_*$ or 0 and whether $I_{SM} = g_{SM}$ or 0. Of these, we show three in Fig. 16A, namely a portion of the nullcline for $s(t) = s_*$ and $I_{SM} = 0$ (for which the left knee is cut off in this figure), the nullcline for $s(t) = s_*$ and $I_{SM} = g_{SM}$, and a portion of the nullcline for $s(t) = 0$ and $I_{SM} = g_{SM}$ (which is no longer cubic and which appears in the lower right of the figure).

The thalamic cells respond whenever a sensorimotor input arrives ($I_{SM} = g_{SM}$) with $s(t) = 0$. An example of this is the first spike **1** in Fig. 16A. Since $s(t) = 0$ when this occurs, the trajectory jumps up all the way to the $s(t) = 0$, $I_{SM} = g_{SM}$ nullcline. When sensorimotor input arrives with $s(t) = s_*$, the thalamic cells may or may not respond, depending on whether w is above the left knee of the nullcline corresponding to $I_{SM} = g_{SM}$ and $s(t) = s_*$. The structure labeled **2** in Fig. 16A shows an example of a response to an input that arrives with $s(t) = s_*$ and is blocked by the left branch of the $s(t) = s_*$, $I_{SM} = g_{SM}$ nullcline. Note that after **2**, the trajectory returns to the left branch of the $s(t) = s_*$, $I_{SM} = 0$ nullcline, because the inhibition remains on (Fig. 16B, dashed curve). The structure labeled **3** in Fig. 16A is

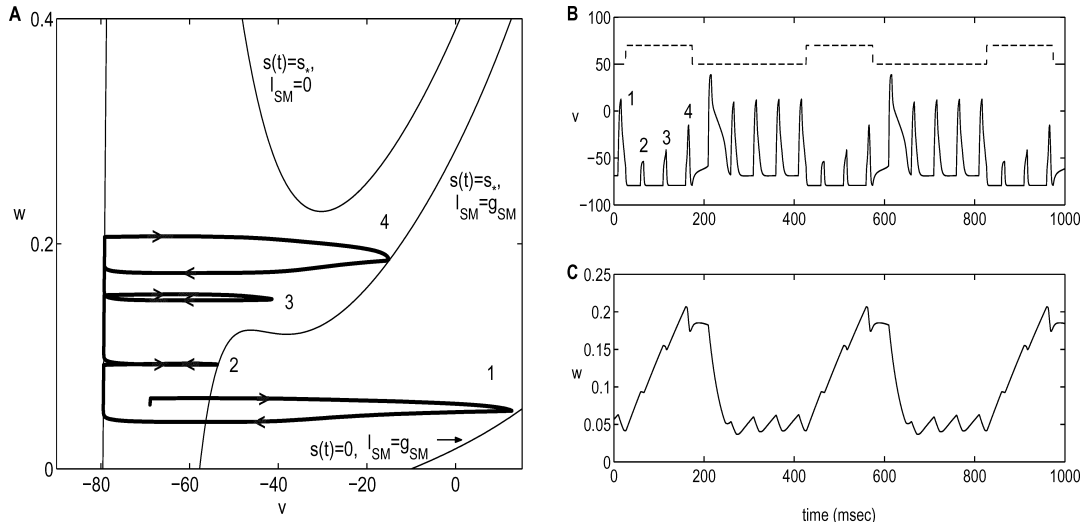

Figure 16. TC response to excitatory inputs in the parkinsonian case. Parameters of I_{SM} are as in Fig. 14A. A: w versus v for the solution shown in the bottom row of Fig. 14A, which is shown again in B here. The plot in A includes three v-nullclines, corresponding to different values of inhibition s and depolarizing input as labeled. The numbered structures in A correspond to responses to the first four inputs. B: v versus times (solid curve), with the same four inputs numbered as in A, together with the time course of the inhibition to the TC cell (dashed line). C: w versus time for this same solution.

not fully blocked, but is close enough to the knee of the $s(t) = s_*$, $I_{SM} = g_{SM}$ nullcline to be only a partial response; if the excitatory input had lasted longer, then this would have been a full response. The structure labeled **4** is a full response with $s(t) = s_*$, in this case, when the excitatory input arrives, w is sufficiently large to allow a full jump up to the right branch of the $s = s_*$, $I_{SM} = g_{SM}$ nullcline. As observed in Fig. 16B, the full response **4** in the presence of inhibition is not as large as those during pauses in inhibition. This corresponds to the fact that the right branch of the nullcline with $s = s_*$, $I_{SM} = g_{SM}$ lies at less depolarized values of v than the $s = 0$; $I_{SM} = g_{SM}$ nullcline, as seen in Fig. 16A.

There is a second, more subtle and perhaps even more important feature contributing to the block of thalamic responsiveness in the parkinsonian case. It is apparent from Fig. 16 that even after the fourth response ends, w, which represents availability of the T-current, is still quite large; this is evident in particular from the time course of w in Fig. 16C. After this occurs, inhibition turns off (dashed line in the top row of the right panel, translated for visibility), and the thalamic response to the next excitatory input, occurring just after time 200 msec, is particularly exaggerated. During this exaggerated response, w decays, inactivating the T-current. While the inactivated level of w does not block responses to subsequent inputs with $s = 0$ (times 200–400 msec in Fig. 16B), which resemble structure **1** in the TC phase space in Fig. 16A, w remains low during these inputs (Fig. 16C). This inactivation prevents the TC cell from responding to the first input that arrives after the inhibition is restored (after time 400 msec in Fig. 16B), and the resulting trajectory in phase space is similar to structure **2** in Fig. 16A.

4.6. Full Model

In the reduced model, we eliminate sodium and potassium currents, and in fact thalamic responses are entirely due to the calcium T-current. This may seem to be at odds with our simulations of the full network, with the full thalamic cell model (1), in which sodium spikes are included and in which the bursts to which calcium contributes represent pathological responses. We shall see in this subsection, however, that the role of the inactivation of the sodium current in the full model is directly analogous to the role played by the inactivation of the T-current in the reduced model in all three cases. In the parkinsonian case in particular, insufficient deinactivation of the T- and sodium currents at the onset of an epoch of phasic inhibition can lead to failed responses in the reduced and full models,

respectively. Further, excessive deinactivation of these currents at the end of an inhibitory epoch can contribute to a pathologically prolonged response in both models, although in the full model, the excessive sodium deinactivation is coupled with T-current deinactivation and leads to a burst of spikes that the reduced model cannot replicate.

We now consider the full network simulations, with thalamic cells modeled by (1). In both normal and DBS conditions, simulations show that the T-current availability, quantified by the inactivation variable r_{Th} in Eq. (1), remains roughly constant. If we average over the inhibitory input from GPi to TC and assume that r_{Th} is constant, then Eq. (1) reduces to a two-dimensional system, the dynamics of which can be viewed in the $(v_{\mathrm{Th}}, h_{\mathrm{Th}})$ phase plane.

Under these simplifications, it is useful to consider the bifurcation structure of the equilibria of Eq. (1), occurring at the intersections of the v_{Th} and h_{Th}-nullclines, taking either the excitatory input I_{SM} or r_{Th} as the bifurcation parameter.

Figure 17A shows a bifurcation diagram for Eq. (1) with I_{SM} as a bifurcation parameter, with $g_{\mathrm{GPi}\to\mathrm{Th}} s_{\mathrm{GPi}} = 0.15$ and $r_{\mathrm{Th}} = 0.05$, corresponding to the normal case. This diagram was generated by starting with $I_{\mathrm{SM}} = 0$, which is marked by the leftmost arrow

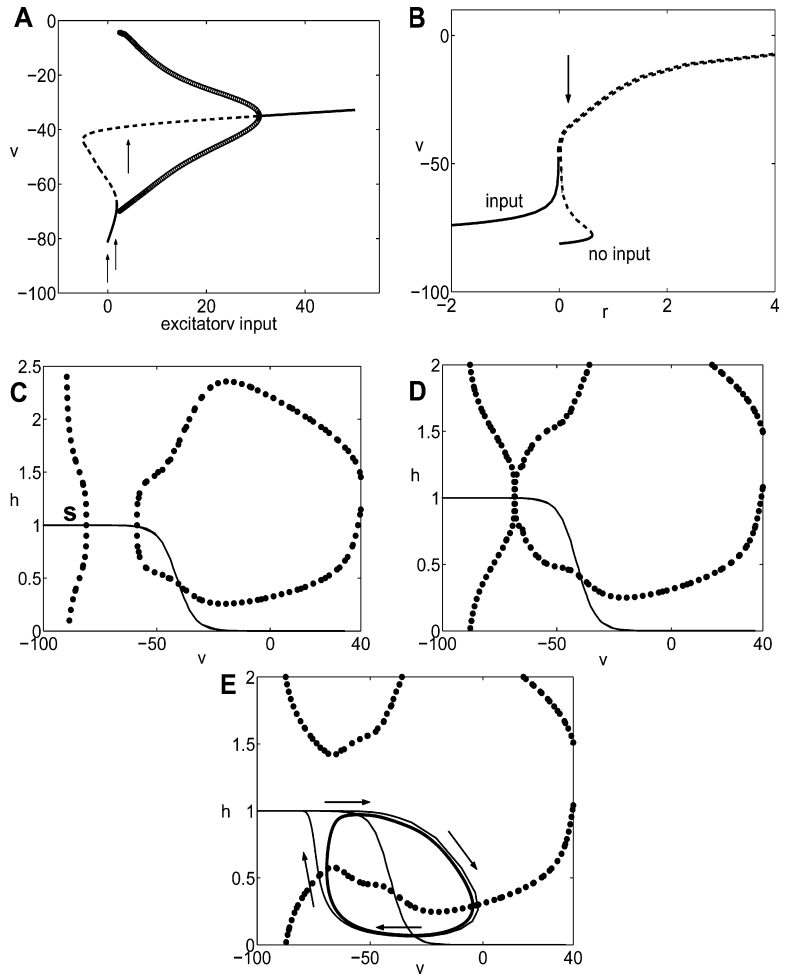

Figure 17. Bifurcation diagrams and nullclines for the full model in the normal case with $g_{\mathrm{GPi}\to\mathrm{Th}} s_{\mathrm{GPi}}$, r_{Th}, and I_{SM} as parameters. In A and B, solid curves are stable equilibria while dashed curves are unstable. The curves of open circles in A delineate a family of stable periodic orbits. In C–E, the solid curve is the h_{Th}-nullcline and the thick dotted curve is the v_{Th}-nullcline; the subscript Th is omitted in the diagrams. $I_{\mathrm{SM}} = 0$, 1.84, 3 in C–E, respectively. In E, the looped curve is a response to a transient excitatory input, with the direction of flow shown by the arrows, and the thicker closed curve is a stable periodic orbit.

in Fig. 17A, and following the curve of equilibria of (1). Note that pairs of equilibria coalesce at two points in this diagram, one with negative I_{SM} and the other, a saddle-node bifurcation point, with $I_{SM} \approx 1.84$, indicated by the middle arrow in Fig. 17A. In addition to stable (solid curve) and unstable (dashed curve) equilibria, the bifurcation diagram shows the envelope of a family of periodic orbits of (1), marked by open circles, which are generated by a Hopf bifurcation through which the unstable equilibrium of (1) stabilizes, as I_{SM} increases to very large values.

For $I_{SM} = 0$, there are three equilibria, two of which are unstable; the corresponding nullclines of (1) are shown in Fig. 17C, where the stable critical point is marked with an **s**. In the absence of input, a TC cell with $g_{GPi\to Th}s_{GPi} = 0.15$ and $r_{Th} = 0.05$ will approach this stable critical point. At $I_{SM} \approx 1.84$, as noted above, two of these equilibria coalesce in a saddle node bifurcation, marked by the middle arrow in Fig. 17A. The corresponding nullclines are shown in Fig. 17D. For $I_{SM} > 1.84$, Eq. (1) has only a single unstable equilibrium along with a stable periodic orbit. An example of the nullclines and the stable limit cycle for this scenario, with $I_{SM} = 3$ (marked by the rightmost arrow in Fig. 17A), is shown in Fig. 17E. When an excitatory input $I_{SM} > 1.84$ arrives, since there is no longer a stable critical point, a TC cell that had been at rest will respond with its own increase in v_{Th} and approach the stable periodic orbit. This will lead to a spike if I_{SM} is sufficiently large and the input is of sufficiently long duration. Once the input is turned off, the TC cell will return to the stable critical point **s** as shown in Fig. 17E. Note that if the duration of the elevated input is too long, then the TC cell will generate multiple spikes as the solution tracks close to the stable limit cycle.

Figure 17B shows the bifurcation diagram for (1) in the normal case again, but with r_{Th} as a bifurcation parameter. The arrow marks the level near which r_{Th} remains throughout our simulations, which was used to generate Fig. 17A and C–E. The two bifurcation curves in Fig. 17B correspond to $I_{SM} = 0$, labeled "no input", and $I_{SM} = 8$, labeled "input". At the relevant level of r_{Th}, an input of $I_{SM} = 8$ switches the nullclines of the TC cell from the configuration in Fig. 17C to that in Fig. 17E, allowing the TC cell to leave the silent phase. Figure 17B illustrates that a qualitatively similar elimination of the stable fixed point by excitatory input would arise over an interval of r_{Th} levels.

Figure 18 shows analogous bifurcation diagrams and nullcline intersections for the DBS case, with $g_{GPi\to Th}s_{GPi} = 0.45$ and $r_{Th} = 0.15$, as observed in a sample simulation. The sets of nullclines in Fig. 18C–F correspond to the four points labeled by arrows in Fig. 18A, with $I_{SM} = 0$, 5, 6, and 8, respectively. The arrow in Fig. 18B shows the level of r_{Th} used in Fig. 18A and C–F and indicates that qualitatively similar results would occur over a large interval of r_{Th}. Note that as I_{SM} increases in Fig. 18A, the unstable equilibrium of (1) stabilizes through a Hopf bifurcation, which generates a family of stable periodic orbits. This is identical to the normal case, although the Hopf occurs at much lower input levels under DBS. The stable periodic orbit for $I_{SM} = 8$ is shown in Fig. 18F; An example of a trajectory generated by a response to an excitatory input $I_{SM} = 8$ is shown in Fig. 18F.

The most complicated scenario in the full model is the parkinsonian case, where $g_{GPi\to Th}s_{GPi}$ and r_{Th} vary rhythmically. The nullclines of Eq. (1) with four different sets of ($g_{GPi\to Th}s_{GPi}$, r_{Th}) values are shown in Fig. 19. In each diagram, the v_{Th}-nullcline is shown both with input off ($I_{SM} = 0$) and with input on ($I_{SM} = 8$). Starting from a baseline of no inhibition and $r_{Th} = 0$, such that the T-current is completely inactivated (see below), we see in Fig. 19A that an excitatory input eliminates a stable rest state, allowing a response unless the excitatory input is extremely brief. Once inhibition turns on, to a level typically seen in parkinsonian simulations, an excitatory input is no longer sufficient to eliminate the stable equilibrium and allow a response (Fig. 19B). Eventually, the T-current builds up (i.e., r_{Th} increases), such that the same excitatory input becomes sufficient to allow a response, as shown in Fig. 19C; this is analogous to moving to larger values of r_{Th} in Fig. 17B or Fig. 18B, where the stable equilibrium (on the curve with input) is lost. This result suggests that faster T-current deinactivation would improve TC responsiveness in the parkinsonian case.

The T-current remains available until the inhibition wears off; however, once this occurs, the stable equilibrium does not exist even with the input off (as on the "no input" curve in Figs. 7B, and 18B, for sufficiently large r_{Th}), and thus a burst of spikes can occur until the T-current inactivates sufficiently. Faster T-current inactivation would shorten or eliminate bursting. The thorough T-current inactivation during a burst, following the removal of inhibition, returns the TC cell to the state illustrated in Fig. 19A, however. As we have just discussed, this will lead to loss of faithful responses when inhibition returns, unless T-current deinactivation could be somehow accelerated.

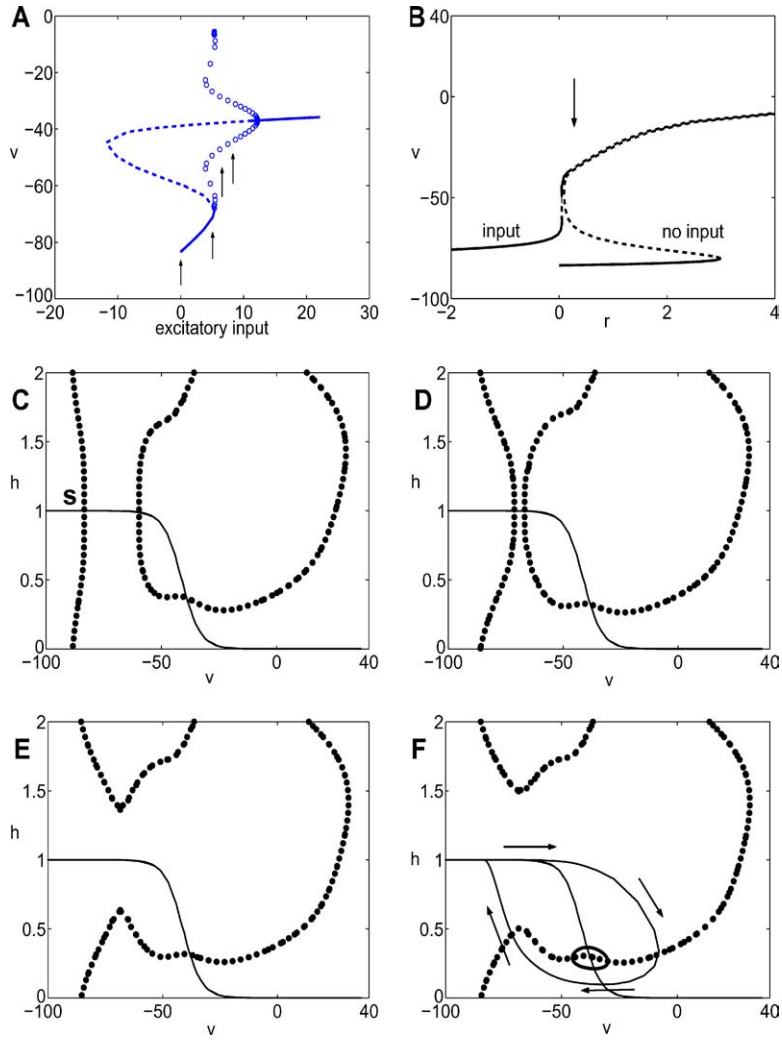

Figure 18. Bifurcation diagrams and nullclines for the full model in the DBS case with $g_{\mathrm{GPi}\to\mathrm{Th}}s_{\mathrm{GPi}}$, r_{Th}, and I_{SM} as parameters. Curve types are as in Fig. 17. $I_{\mathrm{SM}} = 0, 5, 6, 8$ in C–F, respectively. A stable periodic orbit is shown as the small, solid closed curve in F. The larger loop in F is a trajectory generated in response to a transient of excitatory input, with the direction of flow shown by the arrows.

5. Discussion

In this paper, we use a computational model to consider how DBS of the STN may affect firing patterns in the basal ganglia and in some of the cells targeted by basal ganglia outputs. Our simulations and analysis support the paradoxical-seeming idea that DBS may enhance the firing rate of inhibitory GPi cells, and that this may actually *improve* the responsiveness to excitatory inputs of the TC cells that GPi targets. More specifically, we find that the increased rhythmicity of STN and GPe firing in parkinsonian conditions leads to rhythmic GPi firing, and thus *phasic* inhibition of TC cells, which can induce bursting and compromise TC responsiveness. High-frequency stimulation induces high-frequency, tonic firing of GPi, which results in strong but *tonic* inhibition of TC cells. This tonic inhibition may have a much weaker effect on TC responsiveness, through mechanisms that our simulations and analysis explain. Thus, the key point of our results is that DBS may be effective at reducing motor symptoms of parkinsonism because it eliminates the oscillatory nature of the inhibition to TC cells. Although this argument runs counter to much of the existing theorization on what mechanisms underlie the efficacy of DBS, it

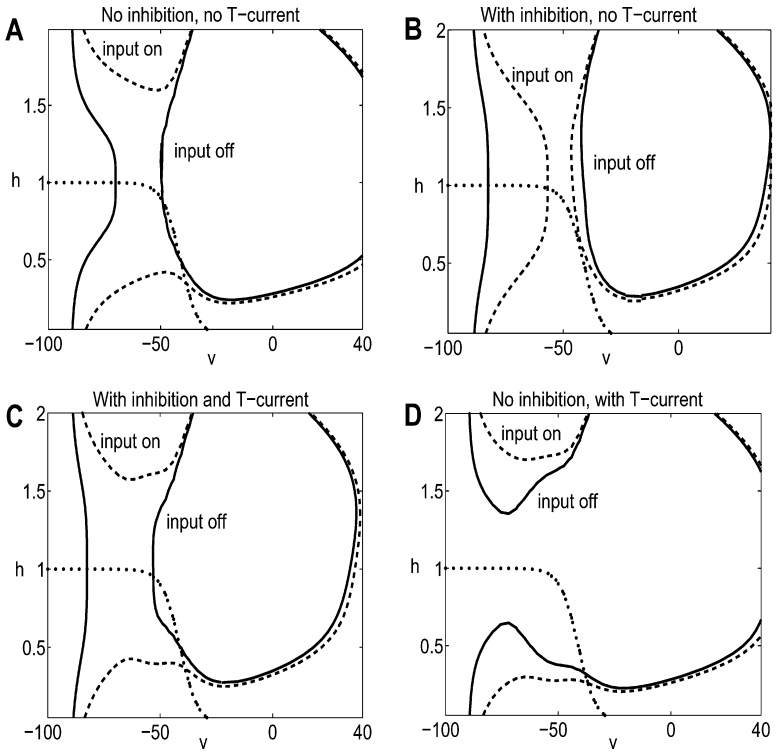

Figure 19. Nullclines for the full model in the parkinsonian case with $g_{\mathrm{GPi}\to\mathrm{Th}}s_{\mathrm{GPi}}$, r_{Th}, and I_{SM} as parameters. Specifically, $g_{\mathrm{GPi}\to\mathrm{Th}}s_{\mathrm{GPi}} = 0$ for no inhibition and 0.2625 with inhibition; $r_{\mathrm{Th}} = 0$ for no T-current and 0.06 with T-current; and $I_{\mathrm{SM}} = 0$ for input off (solid) and 8 for input on (dashed). The h-nullcline is dotted.

is quite natural from the perspective of oscillatory networks.

A variety of possible mechanisms to explain the therapeutic effects of DBS of STN are reviewed in, for example (Ashby et al., 2000; Benazzouz et al., 2000; Montgomery and Baker, 2000; Obeso et al., 2000; Benabid et al., 2001c,d; Dostrovsky et al., 2002; Vitek, 2002). Several of these rely on the idea that DBS somehow silences STN firing (Obeso et al., 2000; Benabid et al., 2001c,d; Beurrier et al., 2001; Levy et al., 2001). Recordings have been done in the basal ganglia of rats and monkeys to assess how high-frequency stimulation (HFS) affects neuronal activity. Benazzouz et al. (1995, 2000) found that HFS of STN in rats suppresses activity of cells in pallidal areas, as well as near the stimulation site in STN. These studies compare firing before HFS with that after HFS, however; thus, they do not establish how firing changes during HFS. Indeed, it is quite possible that after a period of sustained, high-frequency STN firing, STN activity will be suppressed by the activation of a calcium-gated potassium afterhyperpolarization current (Bevan et al., 1999, 2000; Terman et al., 2002).

Alternatively, many recent experimental results support the contrasting view that HFS of STN may in fact lead to high-frequency firing in GPi. It is possible that this occurs directly through high-frequency STN activity, as in our model, which is consistent with the fact that STN cells can fire at several hundred Hz in response to sustained applied currents (Bevan et al., 1999, 2000). Indeed, Garcia et al. (2003) recently used spike-sorting and stimulus artifact removal techniques to distinguish that at frequencies relevant to DBS, HFS of STN leads to STN spikes time-locked to stimulus pulses, blocking altered parkinsonian activity. Although individual STN cells stopped firing after some activity period in these experiments, presumably average activity over the STN population resembled that of our model cells. Alternatively, it is possible that high-frequency GPi activity develops under HFS of STN because HFS drives the efferent axons projecting from the site where it is applied, augmenting neurotransmitter release, as argued by Montgomery and Baker (2000). It has been

shown, for example, that HFS of STN in normal rat leads to an increase in extracellular glutamate in GPi and the substantia nigra pars reticulata (SNr), to which STN is the primary source of excitatory afferents (Paul et al., 2000; Windels et al., 2000). This theory is also supported by studies in parkinsonian patients, which found inhibitory effects after microstimulation of GPi (Dostrovsky et al., 2000), as well as increases in blood oxygenation level-dependent signal in subcortical regions in functional magnetic resonance imaging during DBS of STN, suggesting overstimulation of STN targets (Jech et al., 2001). More recently, from direct recording with spike-sorting and stimulus artifact removal, HFS of STN was found to increase the mean discharge rate of GPi and GPe cells, with GP firing becoming synchronized to the stimulus (Hashimoto et al., 2003), and that the primary effect of HFS of GPi is to inhibit neuronal spikes in thalamic targets of GPi (Anderson et al., 2003). Finally, this idea is borne out in experimental (Nowak et al., 1998a,b) and computational (McIntyre et al., 1999) studies showing that electrical stimulation of extracellular gray matter activates the axons or initial segments, rather than the cell bodies, of affected neurons. In summary, regardless of changes in STN activity during DBS, GPi activity appears to increase. Our simulations achieve elevated GPi firing during DBS through high-frequency STN spiking; however, our results do not require actual spiking of STN cells, just that GPi firing becomes faster and more regular during DBS. Indeed, we exploit this fact in our reduced model analysis.

We have proposed that increased, regularized GPi activity during DBS of STN actually allows for normal thalamic responses, because the resulting tonic inhibition to TC cells does not induce the low-thresold calcium rebound bursts that we observe in the parkinsonian state (and which have been observed experimentally to result from pauses in high-frequency SNr firing, Deniau and Chevalier, 1985). Previous authors have also suggested that DBS of STN disrupts pathological patterns or over-synchronization of GPi activity (Ryan et al., 1993; Obeso et al., 1997; Montgomery and Baker, 2000; Obeso et al., 2000; Vitek et al., 2000, 2002; Benabid et al., 2001c). Note that while theories of DBS ecacy that rely on GPi suppression may fail to explain why DBS does not cause serious dyskinesias, the idea that DBS replaces phasic with tonic firing patterns in GPi and elsewhere immediately obviates this issue. Moreover, the idea that DBS works by regularizing basal ganglia output activity is consistent with recent results suggesting that rhythmicity of basal ganglia firing emerges and plays a crucial role in PD (e.g., Nini et al., 1995; Brown et al., 2001; Plenz et al., 1999; Montgomery and Baker, 2000; Brown et al., 2001; Terman et al., 2002). A related idea is that demand-controlled, low-frequency stimulation may offer a milder means of eliminating pathological STN synchronization and associated motor symtoms (Tass, 2002). A primary contribution of our study is that we elucidate a specific mechanism that could explain why parkinsonian firing patterns lead to negative motor outcomes and why the disruption of these pathological patterns by high-frequency DBS of STN, through its effects on GPi in particular, might restore normal processing of motor programs.

In this context, it is important to note recent evidence that the inhibitory inputs from the basal ganglia to the thalamus do not likely serve to drive the thalamus when it operates in tonic mode, as it will in normal, awake conditions (Smith and Sherman, 2002). Rather, inhibitory inputs would act to modulate other inputs to the thalamus, perhaps corresponding to sensorimotor signals. Thus, parkinsonian conditions that interfere with thalamic responsiveness, for example by causing rhythmic rebound bursts, would compromise the flow of these other inputs through thalamus to cortex, and perhaps even induce a pathological inhibitory drive of the thalamus (Smith and Sherman, 2002). Interventions such as DBS would achieve success by eliminating pathological effects of inhibition and restoring the normal signal flow.

We have not specified the source of the excitatory sensorimotor signals in our study. It is quite reasonable that inhibitory GPi outputs and excitatory corticothalamic projections impinge on common thalamic relay areas. A direct interaction of GPi inhibition and ascending motor signals is suggested by experiments reporting some overlap between the thalamic targets of the GPi and of the cerebellum (Macchi et al., 1997; Mason et al., 2000; Sakai et al., 2000, 2002); however, this notion appears to be controversial. Alternatively, it is possible that rebound bursts induced in one thalamic area by parkinsonian rhythmicity in GPi could themselves trigger bursts in inhibitory thalamic reticular cells (RE), which would in turn induce bursting in TC cells throughout the thalamus, as observed in sleep spindles (e.g., Steriade et al., 1997). The direct projection from GPe to RE also provides a route by which pathological rhythmicity could spread throughout the thalamus. In both of these cases, which we have

not explored, our results suggest that the elimination of rhythmicity through DBS of STN would restore normal thalamic and cortical processing of sensorimotor inputs. While there is significant evidence that basal ganglia and cerebellar inputs to thalamus converge in cortical motor areas (Limousin et al., 1997; Hoover et al., 1999; Middleton et al., 2000; Bergman et al., 2002; Sestini et al., 2002), testing cortical responses to converging thalamic bursts induced by GPi, together with normal signals relayed from the cerebellum through other thalamic nuclei, remains an important step for future simulations and experiments.

In addition to omitting RE cells from our model, we have made numerous other assumptions. In particular, we have assumed that the role of the GPi is simply to relay input from STN, and we have not considered how the basal ganglia might play a functional role in modulating sensorimotor signals to the thalamus. Further, we have neglected certain connections within the basal ganglia, such as those from striatum to GPi. We have also taken an extremely simplistic view of the effect of DBS on neuronal activity, ignoring, for example, any field effects or variations due to the differential positioning of a stimulating electrode relative to different cells that it affects. Finally, we have treated individual cells as single compartment units. Nonetheless, the mechanism that we have elucidated is based on a small number of properties, such as rhythmicity of indirect pathway activity in PD and TC rebound burst firing in response to phasic inhibition, that have been experimentally observed in basal ganglia and TC cells and that do not depend on the specifics of our approach.

We conclude by pointing out several predictions associated with our results. Our fundamental prediction is that in PD, rhythmic rebound bursts associated with the low-threshold calcium T-current occur in TC cells and possibly in cortical motor areas, at least during time periods when the basal ganglia is firing rhythmically. These bursts are predicted to be drastically reduced under DBS. Further, we expect that firing in at least one of GPi and GPe speeds up and regularizes in DBS, relative to PD or normal states, and that there is an increase in correlated firing of GPi with GPe under DBS (and with STN, if STN cells are still firing). If GPi speed up and regularization is observed, then we can further predict that GPe lesion will not compromise the effectiveness of DBS of STN, although this is more ambiguous, due to the pathway from GPe to RE as noted above. Finally, although the presence of multiple pathways again clouds the issue, it would be expected that blockage of bursts or regularization of firing in ventral lateral thalamic areas (and other thalamic nuclei targeted by GPi) should have some therapeutic effect for PD, as is known (see review in Olanow et al., 2000, 2001) to be attained through DBS of the ventral intermediate thalamic nucleus.

Appendix

Here we describe the parameters and nonlinear functions used for each cell type and for the synaptic coupling.

For the thalamic neurons, given by (1), we let $g_L = .05$, $E_L = -70$, $g_{Na} = 3$, $E_{Na} = 50$, $g_K = 5$, $E_K = -90$, $g_T = 5$, $E_T = 0$, $h_\infty(v) = 1/(1 + \exp((v + 41)/4))$, $r_\infty(v) = 1/(1 + \exp((v + 84)/4))$, $\tau_h(v) = 1/(a_h(v) + b_h(v))$, $a_h(v) = .128\exp(-(v + 46)/18)$, $b_h(v) = 4/(1 + \exp(-(v + 23)/5))$, $\tau_r(v) = (28 + \exp(-(v + 25)/10.5)))$, $m_\infty(v) = 1/(1 + \exp(-(v + 37)/7))$, $p_\infty(v) = 1/(1 + \exp(-(v + 60)/6.2))$.

Details of how the STN and GPe neurons are modeled can be found in Terman et al. (2002). Slight parameter changes were made to compensate for the fact that the model in Terman et al. (2002) was based on *in vitro* data. In particular, STN cells were given an applied current of 25 pA/μm^2, while GPe cells were given an applied current of 2 pA/μm^2. Further, the dimensionless calcium decay rate k_{Ca} in GPe cells was lowered from 20, as reported in Terman et al. (2002), to 15, and the dimensionless potassium channel activation rate ϕ_n was raised from 0.05 to 0.1. In our simulations there were sixteen STN neurons and sixteen GPe neurons. Each STN neuron received inhibitory input from two GPe neurons. Each GPe neuron received excitatory input from three STN neurons and inhibitory input from two other GPe neurons. The GPi neurons were modeled exactly as the GPe neurons, with an additional applied current of $I_{app} = 3$ pA/μm^2 to enhance firing. There were sixteen GPi neurons and each of these received excitatory input from one STN neuron. There were two thalamic neurons; each received inhibitory input from eight GPi neurons.

Each synaptic variable s_α satisfies Eq. (5). For $\alpha = $ Gi, Ge, Sn we generally take A_α, B_α, $\theta_\alpha = (2, .08, 20)$, $(2, .04, 20)$, $(5, 1, 30)$. We used distinct kinetic parameters for the synaptic inputs to the GPi cells, however, namely A_{Ge}, $B_{Ge} = (1, .1)$ and A_{Sn}, $B_{Sn} = (1, .05)$. The synaptic currents are of the form $I_{\alpha\to\beta} = g_{syn}S_{tot}(v_\beta - E_{syn})$ where S_{tot} is

the sum of the presynaptic variables. For $I_{Ge\to Sn}$, $I_{Sn\to Ge}$, $I_{Ge\to Ge}$, $I_{Sn\to Gi}$, $I_{Gi\to Gi}$, $I_{Gi\to Th}$, we let $(g_{syn}, E_{syn}) = (.9, -100)$, $(.3, 0)$, $(1, -80)$, $(.3, 0)$, $(1, -100)$, $(.06, -85)$.

The parameters for I_{SM} in Section 3 were $i_{SM} = 5$, $\rho_{SM} = 25$, $\delta_{SM} = 5$. The parameters used for I_{SM} in the reduced model simulations in Section 4 are listed in Fig. 14A. During DBS, we took the following parameters for I_{DBS}: $i_D = 400$, $\rho_D = 12.5$; $\delta_D = 3$.

Acknowledgments

This work was partially funded by NSF grants DMS-0108857 (JER) and DMS-0103822 (DT). We thank Bard Ermentrout for helpful comments on an earlier version of this manuscript. The authors also received funding from the Pittsburgh Institute for Neurodenerative Disease.

References

Albin R, Young A, Penney J (1989) The functional anatomy of basal ganglia disorders. Trends Neurosci. 12: 366–375.

Anderson M, Postpuna N, Ruffo M (2003) effects of high-frequency stimulation in the internal globus pallidus on the activity of thalamic neurons in the awake monkey. J. Neurophysiol. 89: 1150–1160.

Ashby P (2000) What does stimulation in the brain actually do? Prog. Neurol. Surg. 15: 236–245.

Benabid A, Koudsie A, Benazzouz A, Piallat B, Krack P (2001) Deep brain stimulation for Parkinson's disease. Adv. Neurol. 86: 405–412.

Benabid A, Koudsie A, Benazzouz A, Piallat B, Krack P, Blerkom NV, Fraix V, Pollak P (2001) Subthalamic nucleus deep brain stimulation. In Lozano A. ed., Movement Disorder Surgery. S. Karger AG, Basel.

Benabid A, Koudsie A, Benazzouz A, Piallat B, Krack P, Limousin-Dowsey P, Lebas J, Pollak P (2001) Deep brain stimulation for Parkinson's disease. In: Calne D, Calne SM, eds., Advances in Neurology, Vol 86: Parkinson's Disease. Lippincott Williams & Wilkins, Philadelphia.

Benabid A, Koudsie A, Benazzouz A, Vercueil L, Fraix V, Chabardes S, Lebas J, Pollak P (2001) Deep brain stimulation of the corpus luysi (subthalamic nucleus) and other targets in parkinson's disease. Extension to new indications such as dystonia and epilepsy. J. Neurol. 248(Supp. 3): S37–S47.

Benazzouz A, Gao D, Ni Z, Piallat B, Bouali-Benazzouz R, Benabid A (2000) Effect of high-frequency stimulation of the subthalamic nucleus on the neuronal activities of the substantia nigra pars reticulata and the ventrolateral nucleus of the thalamus. Neuroscience. 99: 289–295.

Benazzouz A, Hallett M (2000) Mechanisms of action of deep brain stimulation. Neurology, 55(Supp. 6): S13–S16.

Benazzouz A, Piallat B, Pollack P, Benabid A (1995) Responses of the substantia nigra pars reticulata and globus pallidus complex to high frequency stimulation of the subthalamic nucleus in rats: Electrophysiological data. Neurosci. Lett. 189: 77–80.

Bergman H, Deuschl G (2002) Pathophysiology of Parkinson's disease: From clinical neurology to basic neuroscience and back. Mov. Disord. 17(Suppl. 3): S28–S40.

Bergman H, Wichmann T, Karmon B, DeLong M (1994) The primate subthalamic nucleus. II. Neuronal activity in the MPTP model of parkinsonism. J. Neurophysiol. 72: 507–520.

Beurrier C, Bioulac B, Audin J, Hammond C (2001) High-frequency stimulation produces a transient blockade of voltage-gated currents in subthalamic neurons. J. Neurophysiol. 85: 1351–1356.

Bevan M, Wilson C (1999) Mechanisms underlying spontaneous oscillation and rhythmic firing in rat subthalamic neurons. J. Neurosci. 19: 7617–7628.

Bevan M, Wilson C, Bolam J, Magill P (2000) Equilibrium potential of GABA-A current and implications for rebound burst firing in rat subthalamic neurons in vitro. J. Neurophysiol. 83: 3169–3172.

Brown P, Marsden C (1999) Bradykinesia and impairment of EEG desynchronization in Parkinson's disease. Mov. Disord. 14: 423–429.

Brown P, Oliviero A, Mazzone P, Insola A, Tonali P, Lazzaro VD (2001) Dopamine dependency of oscillations between subthalamic nucleus and pallidum in Parkinson's disease. J. Neurosci. 21: 1033–1038.

DeLong M (1971) Activity of pallidal neurons during movement. J. Neurophysiol. 34: 414–427.

Deniau J, Chevalier M (1985) Disinhibition as a basic process in the expression of striatal functions. II. The striato-nigral influence on thalamocortical cells of the ventromedial thalamic nucleus. Brain Res. 334: 227–233.

Destexhe A, Contreras D, Steriade M (1998) Mechanisms underlying the synchronizing action of corticothalamic feedback through inhibition of thalamic relay cells. J. Neurophysiol. 79: 999–1016.

Dostrovsky J, Levy R, Wu J, Hutchison W, Tasker R, Lozano A (2000) Microstimulationinduced inhibition of neuronal firing in human globus pallidus. J. Neurophysiol. 84: 570–574.

Dostrovsky J, Lozano A (2002) Mechanisms of deep brain stimulation. Mov. Disord. 17(Supp. 3): S63–S68.

Ermentrout B (2002) Simulating, Analyzing, and Animating Dynamical Systems. Philadelphia: SIAM Press.

Filion M, Tremblay L (1991) Abnormal spontaneous activity of globus pallidus neurons in monkeys with MPTP-induced parkinsonism. Brain Res. 547: 142–151.

Gerfen C, Wilson C (1996) The basal ganglia. In: Swanson L, Björklund A, Hökfelt T, eds. Handbook of Chemical Neuroanatomy, Vol. 12: Integrated Systems of the CNS, Part III. Elsevier Science B.V.

Gross C (2001) Stimulation of the globus pallidus internus. In: Lozano A, ed. Movement Disorder Surgery. S. Karger AG, Basel.

Hashimoto T, Elder C, Okun M, Patrick S, Vitek J (2003) Stimulation of the subthalamic nucleus changes the firing pattern of pallidal neurons. J. Neurosci. 23: 1916–1923.

Hoover J, Strick P (1999) The organization of cerebellar and basal ganglia outputs to primary motor cortex as revealed by retrograde transneuronal transport of herpes simplex virus type 1. J. Neurosci. 19: 1446–1463.

Jech R, Urgosik D, Tintera J, Nebuzelsky A, Krakensy J, Liscak R, Roth J, Ruzicka E (2001) Functional magnetic resonance imaging during deep brain stimulation: A pilot study in four patients with Parkinson's disease. Mov. Disord. 16: 1126–1132.

Levy R, Lang A, Dostrovsky J, Pahapill P, Romas J, Saint-Cyr J, Hutchison W, Lozano A (2001) Lidocaine and muscimol microinjections in subthalamic nucleus reverse Parkinsonian symptoms. Brain 124: 2105–2118.

Limousin P, Greene J, Pollak P, Rothwell J, Benabid A, Frackowiak R (1997) Changes in cerebral activity pattern due to subthalamic nucleus or internal pallidum stimulation in Parkinson's disease. Ann. Neurol. 42: 283–291.

Macchi G, Jones E (1997) Toward an agreement on terminology of nuclear and subnuclear divisions of the motor thalamus. J. Neurosurg. 86: 670–685.

Magnin M, Morel A, Jeanmonod D (2000) Single-unit analysis of the pallidum, thalamus, and subthalamic nucleus in parkinsonian patients. Neuroscience 96: 549–564.

Mason A, Ilinsky I, Maldonado S, Kultas-Ilinsky K (2000) Thalamic terminal fields of individual axons from the ventral part of the dentate nucleus of the cerebellum in Macaca mullata. J. Comp. Neurol. 421: 412–428.

McIntyre C, Grill W (1999) Excitation of central nervous system neurons by nonuniform electric fields. Biophys. J. 76: 878–888.

Middleton F, Strick P (2000) Basal ganglia and cerebellar loops: Motor and cognitive circuits. Brain Res. Rev. 31: 236–250.

Montgomery E Jr, Baker K (2000) Mechanism of deep brain stimulation and future technical developments. Neurol. Res. 22: 259–266.

Nini A, Feingold A, Slovin H, Bergman H (1995) Neurons in the globus pallidus do not show correlated activity in the normal monkey, but phase-locked oscillations appear in the MPTP model of parkinsonism. J. Neurophysiol. 74: 1800–1805.

Nowak L, Bullier J (1998a) Axons, but not cell bodies, are activated by electrical stimulation in cortical gray matter: I. Evidence from chronaxie measurements. Exp. Brain Res. 118: 477–488.

Nowak L, Bullier J (1998b) Axons, but not cell bodies, are activated by electrical stimulation in cortical gray matter: II. Evidence from selective inactivation of cell bodies and axon initial segments. Exp. Brain Res. 118: 489–500.

Obeso J, Rodriguez M, DeLong M (1997) Basal ganglia pathophysiology: A critical review. In: Obeso J, DeLong M, Ohye C, Marsden C, eds. Advances in Neurology. Lippincott-Raven Publishers, Philadelphia. vol. 74, pp. 3–18.

Obeso J, Rodriguez-Oroz M, Rodriguez M, Macias R, Alvarez L, Guridi J, Vitek J, DeLong M (2000) Pathophysiologic basis of surgery for Parkinson's disease. Neurology 55 (Supp. 6): S7–S12.

Ogura M, Kita H (2000) Dynorphin exerts both postsynaptic and presynaptic effects in the globus pallidus of the rat. J. Neurophysiol. 83: 3366–3376.

Olanow W, Brin M (2001) In: Calne D, Calne SM, eds. Advances in Neurology, Vol. 86: Parkinson's Disease. Lippincott Williams & Wilkins, Philadelphia.

Olanow W, Brin M, Obeso J (2000) The role of deep brain stimulation as a surgical treatment for Parkinson's disease. Neurology 55, (Supp. 6): S60–S66.

Paul G, Reum T, Meissner W, Marburger A, Sohr R, Morgenstern R, Kupsch A (2000) High frequency stimulation of the subthalamic nucleus in uences striatal dopaminergic metabolism in naive rats. NeuroReport 11: 441–444.

Plenz D, Kitai S (1999) A basal ganglia pacemaker formed by the subthalamic nucleus and external globus pallidus. Nature 400: 677–682.

Pollak P, Fraix V, Krack P, Moro E, Mendes A, Chabardes S, Koudsie A, Benabid A (2002) Treatment results: Parkinson's disease. Mov. Disord. 17 (Supp. 3): S75–S83.

Raz A, Vaadia E, Bergman H (2000) Firing patterns and correlations of spontaneous discharge of pallidal neurons in the normal and tremulous 1-methyl-4-phenyl-1,2,3,6 tetrahydropyridine vervet model of parkinsonism. J. Neurosci. 20: 8559–8571.

Rinzel J (1985) Excitation dynamics: insights from simplified membrane models. Fed. Proc. 44: 2944–2946.

Rizzone M, Lanotte M, Bergamasco B, Tavella A, Torre E, Faccani G, Melcarne A, Lopiano L (2001) Deep brain stimulation of the subthalamic nucleus in Parkinson's disease: effects of variation in stimulation parameters. J. Neurol. Neurosurg. Psych. 71: 215–219.

Ryan L, Sanders D (1993) Subthalamic nucleus lesion regularizes firing patterns in globus pallidus and substantia nigra pars reticulata. Brain Res. 626: 327–331.

Sakai S, Inase M, Tanji J (2002) The relationship between MI and SMA afferents and cerebellar and pallidal efferents in the macaque monkey. Somatosens. & Mot. Res. 19: 139–148.

Sakai S, Stepniewska I, Qi H, Kaas J (2000) Pallidal and cerebellar afferents to presupplementary motor area thalamocortical neurons in the owl monkey: a multiple labeling study. J. Comp. Neurol. 417: 164–180.

Sestini S, di Luzio AS, Ammannati F, DeCristofaro M, Passeri A, Martini S, Pupi A (2002) Changes in regional cerebral blood ow caused by deep-brain stimulation of the subthalamic nucleus in Parkinson's disease. J. Nucl. Med. 43: 725–732.

Smith G, Sherman S (2002) Detectability of excitatory versus inhibitory drive in an integrateand-fire-or-burst thalamocortical relay neuron model. J. Neurosci. 22: 10242–10250.

Sohal V, Huguenard J (2002) Reciprocal inhibition controls the oscillatory state in thalamic networks. Neurocomp. 44: 653–659.

Stanford I, Cooper A (1999) Presynaptic μ and δ opioid receptor modulation of $GABA_a$ IPSCs in the rat globus pallidus in vitro. J. Neurosci. 19: 4796–4803.

Steriade M, Contreras D, Amzica F (1997) The thalamocortical dialogue during wake, sleep, and paroxysmal oscillations. In: Steriade M, Jones E, McCormick D, eds. Thalamus, Elsevier, Amsterdam, Vol. II, pp. 213–294.

Tass P (2002) Effective desynchronization with bipolar double-pulse stimulation. Phys. Rev. E 66: 0362261–0362269.

Terman D, Rubin J, Yew A, Wilson C (2001) Synchronous parkinsonian rhythms in a model for the indirect pathway of the basal ganglia. Neurocomp. 39/40: 973–982.

Terman D, Rubin J, Yew A, Wilson C (2002) Activity patterns in a model for the subthalamopallidal network of the basal ganglia. J. Neurosci. 22: 2963–2976.

The Deep Brain Stimulation for Parkinson's Disease Study Group. (2001) Deep-brain stimulation of the subthalamic nucleus or the pars interna of the globus pallidus in Parkinson's disease. New England J. Med. 345: 956–963.

Traub R, Miles R (1991) Neuronal Networks of the Hippocampus. Cambridge, UK: Cambridge University Press.

Vitek J (2002) Mechanisms of deep brain stimulation: excitation or inhibition. Mov. Disord. 17 (Supp. 3): S69–S72.

Vitek J, Giroux M (2000) Physiology of hypokinetic and hyperkinetic movement disorders: Model for dyskinesia. Ann. Neurol. 47 (4 Supp 1): S131–S140.

Wichmann T, Bergman H, Starr P, Subramanian T, Watts R, DeLong M (1999) Comparison of MPTP-induced changes in spontaneous neuronal discharge in the internal pallidal segment

and in the substantia nigra pars reticulata in primates. Exp. Brain Res. 125: 397–409.

Windels F, Bruet N, Poupard A, Urbain N, Chouvet G, Feuerstein C, Savasta M (2000) Effects of high frequency stimulation of subthalamic nucleus on extracellular glutamate and GABA in substantia nigra and globus pallidus in the normal rat. Eur. J. Neurosci., 12: 4141–4146.

Wu Y, Levy R, Ashby P, Tasker R, Dostrovsky J (2001) Does stimulation of the GPi control dyskinesia by activating inhibitory axons? Mov. Disord. 16: 208–216.

Zhan X, Cox C, Rinzel J, Sherman S (1999) Current clamp and modeling studies of lowthreshold calcium spikes in cells of the cat's lateral geniculate nucleus. J. Neurophysiol. 81: 2360–2373.